Nonlinear optical responses of self-assembled monolayers functionalized with indolino-oxazolidine photoswitches

PCCP

Nonlinear Optical Responses Of Self-Assembled Monolayers Functionalized With Indolino-Oxazolidine Photoswitches

Journal:	*Physical Chemistry Chemical Physics*
Manuscript ID	CP-ART-05-2018-002991.R2
Article Type:	Paper
Date Submitted by the Author:	n/a
Complete List of Authors:	Tonnelé, Claire; University of Bordeaux, Institut des Sciences Moléculaires Pielak, Kornelia; University of Namur, Unité de Chimie Physique Théorique et Structurale Deviers, Jean; University of Bordeaux, Institut des Sciences Moléculaires Muccioli, Luca; Universite de Bordeaux, Institut des Sciences Mol‼ eculaires, UMR 5255; Universita degli Studi di Bologna, Dipartimento di Chimica Industriale "Toso Montanari" Champagne, Benoît; Facultes Universitaires Notre Dame de la Paix, Laboratoire de Chimie Theorique Appliquee Castet, Frederic; Universite de Bordeaux 1, Institut des Sciences Moléculaires, CNRS UMR5255

Article type: Full paper

Website www.rsc.org/pccp
Impact factor* 4.123

Journal expectations To be suitable for publication in *Physical Chemistry Chemical Physics* (*PCCP*) articles must include significant new insight into physical chemistry.

Article type: Full paper Original scientific work that has not been published previously. Full papers do not have a page limit and should be appropriate in length for scientific content.

Journal scope Visit the *PCCP* website for additional details of the journal scope and expectations.

PCCP is an international journal for the publication of cutting-edge original work in physical chemistry, chemical physics and biophysical chemistry. To be suitable for publication in *PCCP*, articles must include significant new insight into physical chemistry; this is the most important criterion that reviewers should judge against when evaluating submissions. Example topics within the journal's broad scope include:

- Spectroscopy
- Dynamics
- Kinetics
- Statistical mechanics
- Thermodynamics
- Electrochemistry
- Catalysis
- Surface science
- Quantum mechanics
- Theoretical research

Interdisciplinary research areas such as polymers and soft matter, materials, nanoscience, surfaces/interfaces, and biophysical chemistry are also welcomed if they demonstrate significant new insight into physical chemistry.

Reviewer responsibilities Visit the Reviewer responsibilities website for additional details of the reviewing policy and procedure for Royal of Society of Chemistry journals.

When preparing your report, please:

- Focus on the originality, importance, impact and reliability of the science. English language and grammatical errors do not need to be discussed in detail, except where it impedes scientific understanding.
- Use the journal scope and expectations to assess the manuscript's suitability for publication in *PCCP.*
- State clearly whether you think the article should be accepted or rejected and include details of how the science presented in the article corresponds to publication criteria.
- Inform the Editor if there is a conflict of interest, a significant part of the work you cannot review with confidence or if parts of the work have previously been published.

Thank you for evaluating this manuscript, your advice as a reviewer for *PCCP* is greatly appreciated.

Dr Anna Simpson Executive Editor
Royal Society of Chemistry, UK

Professor Seong Keun Kim Editorial Board Chair
Seoul National University, South Korea

**2016 Journal Citation Reports®, (Thomson Reuters, 2017)*

Journal Name

ARTICLE TYPE

Cite this: DOI: 10.1039/xxxxxxxxxx

Nonlinear Optical Responses Of Self-Assembled Monolayers Functionalized With Indolino-Oxazolidine Photoswitches†

Claire Tonnelé,*[a] Kornelia Pielak,[a,b] Jean Deviers[a], Luca Muccioli[c], Benoît Champagne*[b], and Frédéric Castet*[a]

Received Date
Accepted Date

DOI: 10.1039/xxxxxxxxxx

www.rsc.org/journalname

A computational approach combining molecular dynamic simulations and density functional theory (DFT) calculations is implemented to evaluate the second-order nonlinear optical (NLO) responses of photoresponsive self-assembled monolayers (SAMs) based on indolino-oxazolidine molecular switches. These numerical simulations provide a complete atomistic picture of the morphology of the SAMs, revealing a high degree of positional disorder and an almost isotropic orientation of the chromophores. Subsequent DFT calculations, carried out to evaluate the average first hyperpolarizability of indolino-oxazolidine switches within the SAM, predict that the structural disorder does not significantly reduce the NLO contrast compared to that of the isolated molecules. Chromophores in the SAM can assume a limited number of specific conformers, due to the high rotational barrier that characterize the conjugated bonds along the indolino/oxazolidine-dyene-thiophene sequence. A notable exception is the rotation about the thiophene-thioalkyl bond, which is not only almost free, but also strongly correlated with the magnitude of the first hyperpolarizability. Controlling this rotation by chemical design could thus be a viable strategy to optimize the SAMs NLO response and the performance of photoresponsive devices based on indolino/oxazolidine switches.

1 Introduction

Organic photochromic compounds have been extensively studied in the last decades, owing to their possible integration into a large variety of photonic and optoelectronic applications.[1–3] Surface functionalization with molecular photoswitches yields 2D materials responding to light in a controlled way.[4] One of the most versatile approaches for surface engineering and interface design is to use self-assembled monolayers (SAMs),[5] in which highly efficient and selective "click" reactions can be exploited to introduce a wide range of organic functionalities on well-defined base monolayers, typically consisting in azide-terminated alkylsilanes grafted on commercially available silica substrates.[6–8] Thus, the design of photoresponsive SAMs opens the way for virtually endless materials for applications in optical data storage and signal processing.

While effective in writing the information by switching the chromophores between one (meta)stable state to another, the use of linear absorption spectroscopy to probe the system often results in a destructive readout process, since the state of the photochromic molecules can be altered upon irradiation. Exploiting second-order nonlinear optical (NLO) properties instead provides a strategy for non-destructive readout ability to the system, since NLO responses are revealed using near-infrared wavelengths not energetic enough to trigger uncontrolled photoconversions. Molecules exhibiting large and photoswitchable first hyperpolarizability are thus ideal candidates for photonic technologies with multiple storage and non-destructive readout capacity.[9–11]

Filling the gap between isolated molecular switches and photoresponsive materials nevertheless remains a quite challenging task, which requires anchoring the molecular photochromes on a 2D substrate while preserving i) the reversibility of the switching process, and ii) the NLO responses of the switching states, as well as their contrast. Indeed experiments showing effective

[a] Institut des Sciences Moléculaires (ISM, UMR CNRS 5255), University of Bordeaux, 351 Cours de la Libération, 33405 Talence, France. E-mail: claire.tonnele@u-bordeaux.fr, frederic.castet@u-bordeaux.fr

[b] Unité de Chimie Physique Théorique et Structurale, Chemistry Department, Namur Institute of Structured Matter, University of Namur, Belgium. E-mail: benoit.champagne@unamur.be

[c] Department of Industrial Chemistry "Toso Montanari", University of Bologna, Viale Risorgimento 4, 40136 Bologna, Italy. E-mail: luca.muccioli@unibo.it

† Electronic Supplementary Information (ESI) available: [Force field parameterization; Preparation of the SiO_2 surface; Functionalized surfaces with various coverage rates; Choice of the relevant molecular fragment for NLO calculations; Probability distributions of dihedrals; Relationships between geometrical structures and NLO responses]. See DOI: 10.1039/b000000x/

photoswitchable NLO SAMs based on fulgimide or azobenzene derivatives have been recently reported,[12,13] but addressing the aforementioned challenges from a computational point of view has never been tackled. Yet, by offering a microscopic picture of the relationships between the supramolecular structure and NLO properties of the system, numerical simulations have the potential of providing highly useful guidelines to rationally control the NLO responses of the SAMs.

The present work constitutes a first attempt towards the theoretical design of such complex architectures, focusing on indolino-oxazolidine (IND) compounds anchored onto an amorphous SiO_2 surface. IND derivatives (Scheme 1) exhibit reversible photoconversion between a colorless closed form (CF) and a colored open form (OF) associated with large changes in the first hyperpolarizability.[14–16] To mimic the experimental preparation of indolino-oxazolidine SAMs by click chemistry,[6] IND units were anchored to the silica surface using a two-step process, in which the SiO_2 surface is first grafted with azidoalkyl linkers, and subsequently some of the linkers are functionalized with photoswitchable IND units (Scheme 1). Then, a sequential approach combining classical molecular dynamics (MD) and quantum mechanics (QM) was employed to evaluate the dynamical behavior and second harmonic generation (SHG) responses of the photoresponsive SAMs. MD simulations gave access to the morphology of the NLO-active layer at the atomistic level, and allowed the exhaustive statistical sampling of the multiple geometrical conformations spanned by the chromophores. Finally, DFT calculations performed on individual molecular fragments extracted from the MD trajectories provided a molecular interpretation on how dynamical geometry distortions, induced by thermal and steric effects, impact the SHG responses of both states of the SAM.

2 Theoretical methodology

2.1 Molecular dynamics simulations

As detailed in the electronic supporting information (ESI), modified versions of the General AMBER Force Field[17] (FF) were used to specifically reproduce the equilibrium geometries of the azidoalkyl linkers and of the complete NLO molecule (Scheme 1). Distinct sets of parameters were derived for describing the open and closed forms of IND. Electrostatic potential-fitted (ESP) atomic charges and torsional potentials around the $\theta_1 - \theta_{10}$ dihedrals were calculated at the M06/6-311G(d) level, and inserted in the force field with the methodology described in reference[18]. In addition, since reliable simulations of NLO responses of push-pull systems require an accurate description of the π-electron conjugation,[16] AMBER FF bond lengths were adjusted for both states of the switch so as to closely reproduce DFT bond lengths at the corresponding equilibrium geometries (within a maximum absolute error of 0.006 Å), as well as the bond length alternation (BLA) along the central vinyl bridge (red segments in Scheme 1). The amorphous SiO_2 surface of dimensions 52.044×51.119 $Å^2$ and thickness of about 30 Å was constructed following the scheme described in ESI. IND-functionalized SAMs were subsequently prepared using a strategy mimicking one of the click reactions usually employed experimentally for monolayer modification, namely the Huisgen 1,3-cycloaddition that occurs between an organic azide and an alkyne.[6–8] In a first step, a densely packed SAM of 120 azido-undecylsilane chains, corresponding to a coverage of 4.5 molecules/nm^2, was generated to serve as a basis for grafting the NLO molecules. These long non conjugated linkers are used experimentally to electronically decouple the photochromic units from the substrate. This first sample, referred hereafter to as the "non photoresponsive SAM" (see Scheme 1), was equilibrated for 80 ns keeping fixed the position of the grafting oxygen of each azidoalkyl chain. In the second step, azide terminal groups were replaced by the photochromic compound in its closed form. Since the IND unit is bulkier than the azide unit of the non photoresponsive SAM, only a fraction of azides was replaced, yielding to three samples with different relative IND to total SAM molecule ratios, namely 1/4, 1/2 and 3/4, corresponding to IND coverages of 1.13, 2.26 and 3.38 molecules/nm^2, respectively. The samples were first equilibrated for 30 ns, before we focused on the most dense SAM for which simulation was extended up to 150 ns. Finally, to obtain the open form layer for the highest coverage sample, the force field parameters were switched from the ones optimized for the CF to the ones optimized for the OF for all chromophores simultaneously, thus assuming the complete switching of the SAM layer. The resulting OF system was then equilibrated for further 85 ns.

2.2 Quantum chemical calculations

Individual molecular structures were extracted from the SAM with the highest relative coverage (3/4), at regular intervals along the MD trajectories, and their NLO responses subsequently calculated. Preliminary investigations demonstrated that, in addition to the photoresponsive IND unit, the triazole moiety, and to a lesser extent the alkyl chain, should be explicitly included in the calculations for an accurate evaluation of the hyperpolarizabilities, while the $Si(OH)_2O$ anchoring unit can be omitted (see ESI for details). A total of 900 structures were then used to sample the multiple geometrical conformations adopted by the NLO switches, in both their closed and open forms.

The static and dynamic components of the molecular first hyperpolarizability tensor (β) were calculated using time-dependent (TD) DFT with the M06-2X[19] exchange-correlation functional (XCF) and the 6-311G(d) basis set. As demonstrated in previous theoretical reports, M06-2X is reliable to calculate hyperpolarizabilities of conjugated organic dyes,[20–22] including indolino-oxazolidine derivatives,[16] owing to its substantial amount (54%) of long-range Hartree-Fock exchange. An incident wavelength of 1064 nm, typical of Nd:YAG laser sources, was used in frequency-dependent SHG calculations. The interfacial NLO responses were analyzed by considering the norm of the first hyperpolarizability vector:

$$||\vec{\beta}|| = \beta = \sqrt{\beta_x^2 + \beta_y^2 + \beta_z^2} \quad (1)$$

where the i^{th} component of the β vector is defined from the β tensor elements:

$$\beta_i = \beta_{iii} + \frac{1}{3}\sum_{j \neq i}(\beta_{ijj} + \beta_{jij} + \beta_{jji}) \quad (2)$$

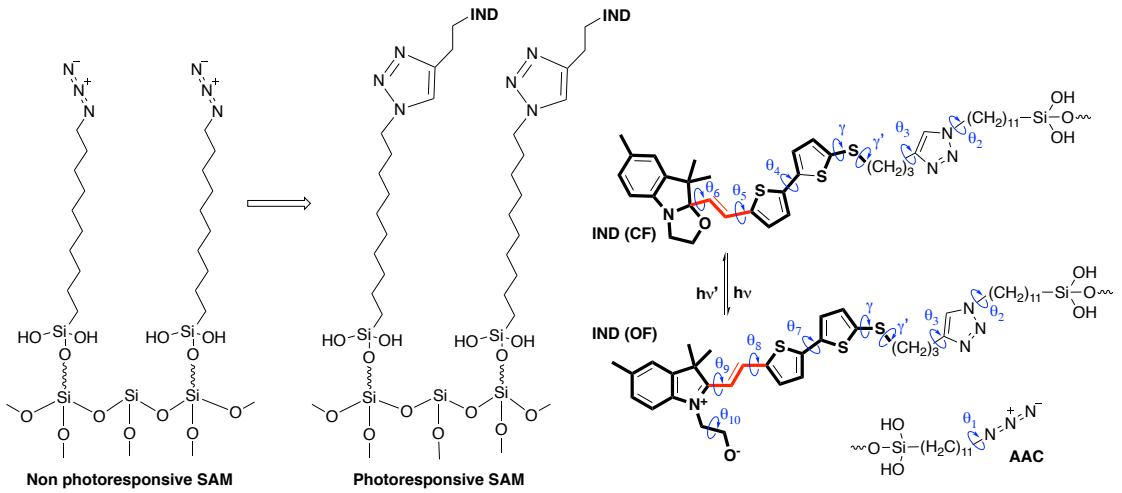

Fig. 1 SiO_2 surface functionalized with azidoalkyl chains (left) and with the photoresponsive molecules (middle). Right: photochromic reaction between the closed form (CF) and open form (OF) of the indolino-oxazolidine derivative (IND, in bold), and azidoalkyl chain (AAC). FF parameters have been derived for torsions θ_1 to θ_{10} (see ESI for the definition of the dihedral angles).

As in the previous work of Tegeder and co.,[12] the anisotropy of the NLO response was also characterized using the component of the β vector normal to the surface plane (β_z), and the corresponding in-plane ones:

$$a = \frac{|\beta_z|}{\sqrt{\beta_x^2 + \beta_y^2}} \quad (3)$$

All calculations were performed using the Gaussian09 package.[23] All β values are reported assuming a Taylor series expansion of the induced dipole with respect to the applied electric field (T convention),[24,25] and are given in atomic units (1 au of $\beta = 3.6310^{-42}$ $m^4V^{-1} = 3.2063 \times 10^{-53}$ $C^3m^3J^{-2} = 8.641 \times 10^{-33}$ esu).

3 Results and discussion

3.1 Morphology of the self-assembled monolayers

The equilibrated morphology of the non photoresponsive SAM (*i.e.* the surface functionalized with azidoalkyl chains only, see Scheme 1), as well as the morphology of the SAM functionalized with the photochromic units in their closed and open forms (for a 3/4 coverage), are represented by the snapshots in Figure 2. The supramolecular organization of the non photoresponsive SAM is characterized by a thickness of 15 ± 2 Å, an average tilt angle of $26 \pm 7°$, a nematic order parameter $\langle P_2 \rangle$ of 0.901 and a roughness of 0.86 Å. To verify the extent of positional order in all SAMs, we used the 2D radial distribution function (RDF) in the (x,y) plane, which gives a measure of the probability of finding a molecule at a given position with respect to a reference central molecule (Figure 3). The 2D RDF of the non photoresponsive SAM clearly evidences a hexagonal positional order in the sample (with a lattice parameter $d = 4.96$ Å), as already observed for H-terminated alkylsiloxane SAMs.[26] Comparing the top panels of Figure 3 reveals that the hexagonal organization of the azidoalkyl layer is globally maintained after functionalization with the photochromic dyes, although it induces a non negligible broadening of the RDF peaks. On the contrary, a visual inspection of the morphology of the photoresponsive SAM (Figure 2) does not evidence any positional order in the top-half sublayer, as confirmed by the 2D RDFs reported in the bottom panels of Figure 3 for the closed and open layers. The distribution of the tilt angle of the dyes with respect to the surface normal (bottom left of Figure 3) reveals that even if a few units are vertically oriented, the distribution is overall almost isotropic. Conversely, the azido-alkyl chains have a uniform, nearly vertical orientation, which is not tilted, unlike that found in the non photoresponsive SAM (cf. top panels of Figure 2).

Decreasing the relative coverage induces a decrease of the SAM thickness, from 40.4 Å (3/4 coverage) to 34.0 Å (1/2 coverage) and 26.7 Å (1/4 coverage). Substantiated by a corresponding increase of the tilt (Table SI-1), this demonstrates how NLO molecules bend at low coverage ratio, while they adopt more elongated conformations in the denser layer. On the other hand, the CF to OF photoconversion does not significantly change the thickness of the SAM (40.4 *vs.* 40.6 Å for CF and OF, respectively). Reversely, the roughness slightly increases when decreasing the coverage, from 1.32 to 3.15 Å.

Focusing on the SAM with higher IND density (3/4 coverage), we investigated more closely the geometrical conformations spanned by the photochromic molecules onto the surface. Consistently with the DFT geometries used for the force field parameterization, the average BLA of the open forms is three times smaller (0.089 ± 0.061 Å) than that of closed forms (0.288 ± 0.061 Å). The distributions of the torsional angles adopted by the molecules within the SAM, plotted with respect to the corresponding rotational potentials of isolated molecules (Figures SI-8 and SI-9), are also informative. Due to high rotation barriers (varying from 3.2 to 13.0 kcal/mol), the population of the $\theta_4 - \theta_{10}$ and γ' dihedrals (Scheme 1) concentrate around the minima of the potential energy curves of the isolated molecules. Reversely, the $\theta_1 - \theta_3$ and γ dihedrals exhibit very broad distributions due to low energy barriers ($\sim$ 1 kcal/mol or smaller). Interestingly, the maxima of the distributions of these torsional angles do not always correspond

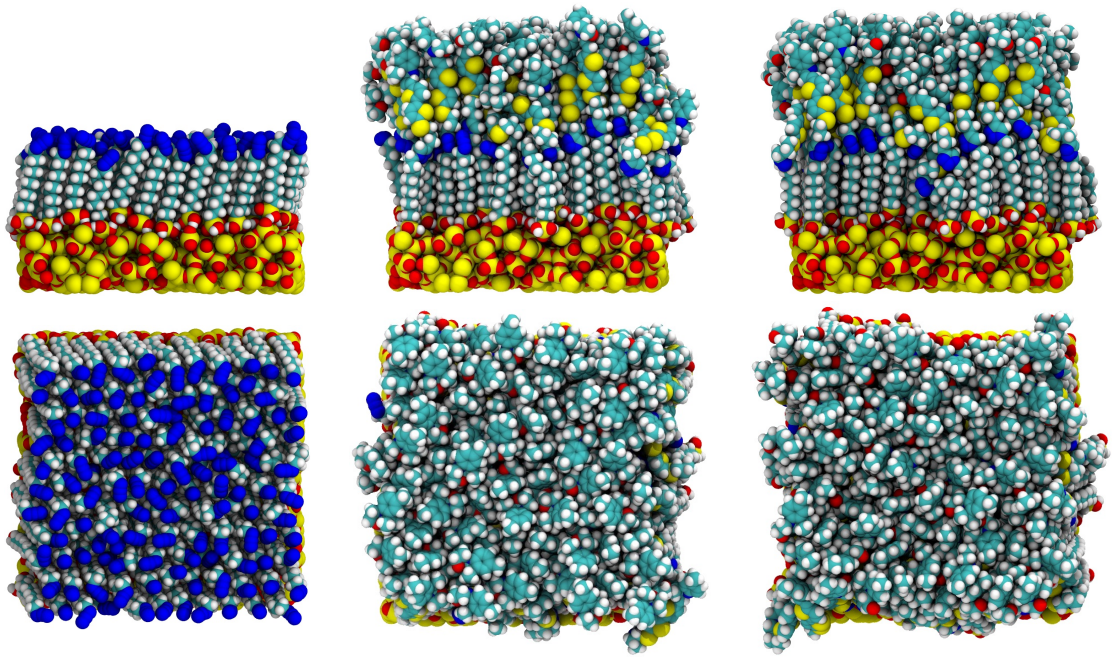

Fig. 2 Left: side and top views of the non photoresponsive SAM. Middle: side and top views of the SAM functionalized with the photochromic units in their closed form. Right: in their open form.

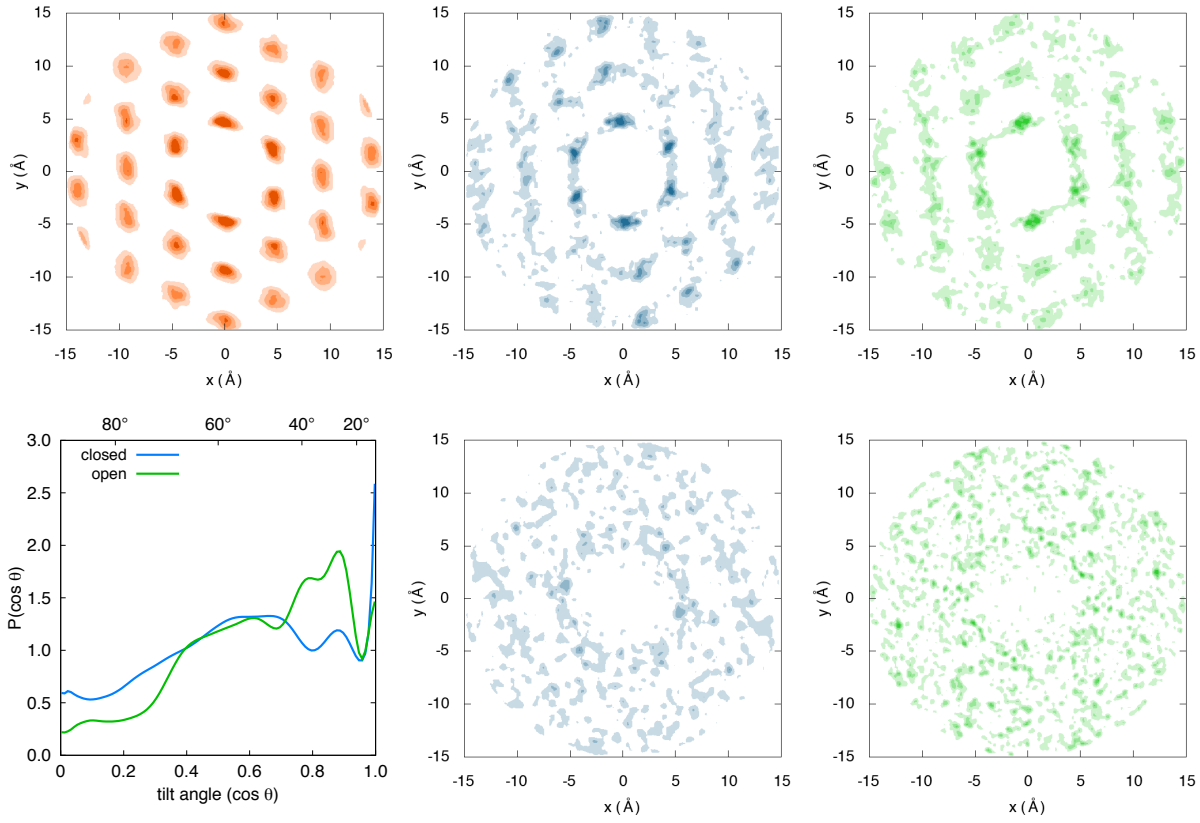

Fig. 3 Top: 2D RDF of the centers of mass of the SAM alkyl chains in the non photoresponsive SAM (left), in the photoresponsive SAM in closed form (middle) and in open form (right). Bottom: distribution of the cosine of the tilt angle θ between the double C=C bond of the vinyl bridge and the axis normal to the surface plane (left), and 2D RDF of the centers of mass of the triazole-indolino-oxazolidine units in the closed and open form SAMs (middle and right panels).

exactly to minima of the potential energy curve, suggesting that the most probable values are dictated by intermolecular interactions.

3.2 Commutation of the nonlinear optical responses

The statistical distributions of the static and dynamic first hyperpolarizabilities (β, eq. 1), of their z-component (β_z), and of the anisotropy factors (a, eq. 3) are illustrated in Figure 4, while average values and standard deviations (σ) are collected in Table 1. The interquartile ranges (IQR), which provide a robust measure of the dispersion of statistical distributions, are also reported.

Considering first the static responses, dynamical geometry fluctuations and steric interactions lead to broad β and β_z distributions, characterized by large σ and IQR values. It also clearly appears from Figure 4 that the distributions of open forms are much broader than those of closed forms, as confirmed by IQR values about four times larger. Moreover for both forms the component normal to the surface plane, β_z, dominates the static hyperpolarizability, as indicated by average anisotropy ratios $\langle a \rangle$ lying between 3.6 and 4.2. Interestingly, a similar $\langle a \rangle$ value ($5.70/\sqrt{2} = 4.03$) was deduced from recent experimental measurements and DFT calculations for the *trans*-configuration of azobenzene-based SAMs.[12] However, while the *trans-cis* isomerization in azobenzene derivatives was shown to strongly reduce the anisotropy of the NLO response owing to the realignment of the upper phenyl ring parallel to the surface, the oxazolidine ring opening in IND derivatives hardly changes the anisotropy of the SHG response, consistently with the invariance of the SAM thickness mentioned above. One also notes that, contrary to the absolute NLO responses, the distribution of the anisotropy ratios is slightly less dispersed for the open form, even if in both cases a considerable fraction of molecules has very low anisotropy, consistently with the broad distributions of tilt angles shown in Figure 3.

The commutation between the closed and open forms induces a large enhancement of the static first hyperpolarizability, as shown by the shift of the β distributions. The OF/CF NLO contrast, evaluated as the ratio between the mean values of the distributions (Table 1), is equal to ~ 7. Strikingly, this contrast is only slightly smaller than the one calculated for the isolated molecule in its equilibrium geometry ($\beta(\mathrm{POF})/\beta(\mathrm{CF}) = 8.93$). This result indicates that, despite the close molecular packing induces strong geometrical distortions, the high degree of disorder of the SAM is not detrimental to the average NLO contrast, which is of crucial importance for device efficiency. This also confirms and extends to amorphous morphologies the conclusions previously deduced from periodic self-consistent charge density functional tight binding calculations, that single IND units anchored through silanol linkers onto a SiO_2 surface maintain their NLO activities and contrasts.[27]

Considering the dynamic NLO responses, the average values of β and β_z computed for the closed forms are enhanced by a factor 2.2 compared to their static analogues. The dynamical distributions are also more dispersed than the static ones, with IQR values about two times larger. In the case of open forms, the dynamic β values are spread over a very broad range, the NLO responses of a few set of structures being strongly contaminated by electronic excitation resonances. In order to rationalize the origin of these resonance effects, the vertical absorption properties of molecular structures exhibiting the lowest and largest dynamic first hyperpolarizabilities were calculated at the M06-2X/6-311G(d) level. The results detailed in ESI show that the large resonance-enhancement arises from the existence of an intense absorption transition close to 532 nm, *i.e.* the second harmonic wavelength of a 1064 nm incident laser beam. These resonance phenomena give rise to numerical instabilities, which make the calculated dynamic β values of the OF less reliable for this particular subset of structures. To partially circumvent this problem, the averages of the dynamic NLO properties of the OF were estimated by considering only the molecules with β values within the interquartile range. For the open form, the enhancement due to frequency dispersion effects, defined as the ratio between the dynamic and static responses, amounts to 7.5 and 3.5 for β and β_z, respectively. Interestingly, the anisotropy of the NLO responses is not impacted by frequency resonance, the average anisotropy ratio $\langle a \rangle$ being identical to that calculated considering the static responses. Finally, the dynamic $\beta(\mathrm{OF})/\beta(\mathrm{CF})$ NLO contrast amounts to ~ 26, *i.e.* more than 3 times the static one, while it is reduced to ~ 13 when considering the z-component only.

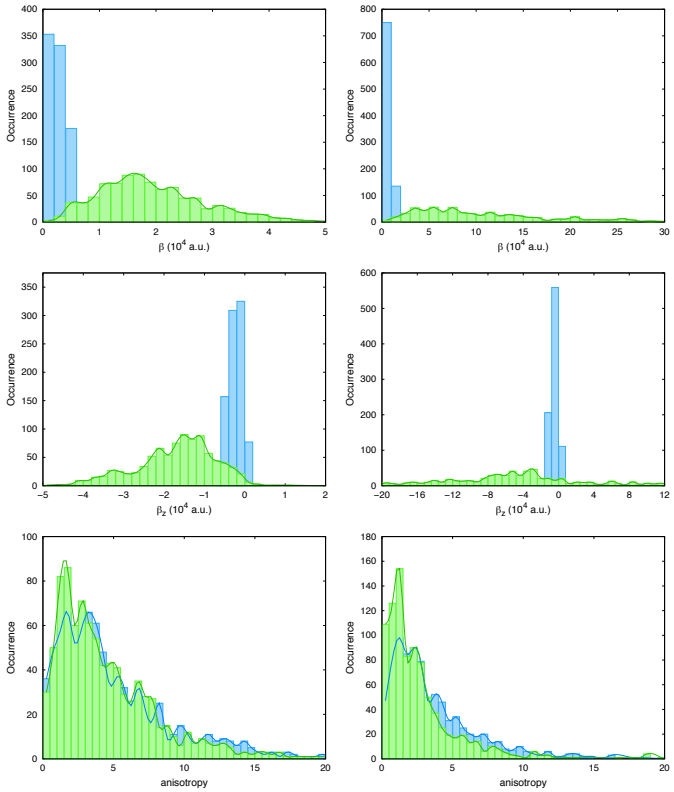

Fig. 4 Distributions of the static (left) and dynamic (right) values of β (top), β_z (middle) and a (bottom), for closed (blue) and open (green) forms.

Table 1 Averaged values, standard deviations (σ), and interquartile range (IQR) of the average static ($\lambda = \infty$) and dynamic ($\lambda = 1064$ nm) hyperpolarizabilities (β), of their z-component (β_z), and of the anisotropy factor (a). The two last lines report the OF/CF enhancement ratios of the NLO responses.

	$\lambda = \infty$		$\lambda = 1064$ nm	
Property	CF	OF	CF	OF
$\langle\beta\rangle \pm \sigma_\beta$	2624 ± 1655	19473 ± 11410	5699 ± 3942	(146337 ± 70035)[a]
$\langle\beta_z\rangle \pm \sigma_{\beta_z}$	-2311 ± 1765	-16725 ± 11322	-4960 ± 4176	(-59100 ± 123161)[a]
$\langle a\rangle \pm \sigma_a$	4.20 ± 5.18	3.56 ± 4.19	4.18 ± 5.22	(3.54 ± 11.09)[a]
IQR(β)	2765	12036	6309	275013
IQR(β_z)	2770	11940	6359	188310
IQR(a)	3.62	3.25	3.66	2.38
$\langle\beta(OF)\rangle/\langle\beta(CF)\rangle$	7.42 ± 9.03		25.68 ± 30.05	
$\langle\beta_z(OF)\rangle/\langle\beta_z(CF)\rangle$	7.24 ± 10.43		11.92 ± 34.86	

[a]Calculated by excluding all the molecules with β values outside the IQR.

3.3 Relationships between geometrical structures and NLO responses

To gain a deeper understanding on the impact of the geometrical distortions on the intrinsic (static) NLO properties of the photochromes, correlations between the calculated β responses and molecular structural parameters were further analyzed. The variations of β with torsional angles around single bonds are reported in ESI, while Figure 5 illustrates the variations of β with respect to γ, as well as to the BLA along the vinyl bridge connecting the indolino-oxazolidine and the bithiophene. As already observed for molecules in solution,[16] Figure 5 (top panel) clearly evidences that the difference in the magnitude of the β response between open and closed forms is mainly driven by the BLA along the central part of the photochromes, whose average value decreases from 0.288 to 0.089 Å. Considering CF and OF separately, it turned out quite unexpectedly that the amplitude of β in both forms is strongly correlated with the value of the torsion angle γ (see Scheme 1). As illustrated in Figure 5 (middle and bottom panels), large first hyperpolarizabilities are obtained for planar conformations with respect to γ (*i.e.* when $\gamma = 0°$ or $180°$), while β is much smaller when the S-C bond of the thiomethylene group is perpendicular to the thiophene ring. Further analyses detailed in the ESI revealed that upon photoexcitation, planar conformations allow the conjugation of one lone pair of the sulfur atom of the thiopropylene, giving rise to an important charge transfer between the sulfur and the dithiophene. This effect is at the origin of the enhancement of the first hyperpolarizability compared to perpendicular conformations. On the contrary, the distributions of β with respect to θ_2 and θ_3 (see ESI) revealed that the amplitude of the NLO responses is not correlated to rotations around these two dihedrals, which also assume all possible values due to low rotational energy barriers. The other dihedrals ($\theta_4 - \theta_{10}$) adopt instead specific values due to conjugation effects and steric constraints.

The striking correlation between the NLO response and the γ torsional angle reveals a crucial effect for the chemical engineering of 2D NLO materials. Owing to the low rotational energy barrier for the rotation around γ (∼0.8 kcal/mol, see ESI), the conformations adopted are mostly driven by intermolecular contacts. Since these packing effects are very difficult to control, it emerges that the best strategy to maximize the NLO responses of dye-

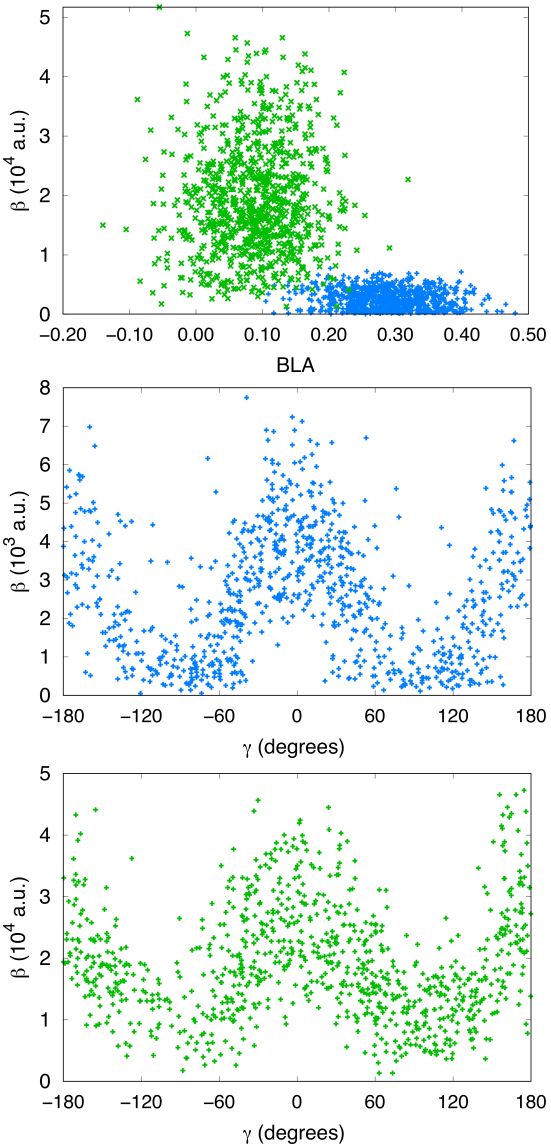

Fig. 5 β values plotted versus the BLA and γ torsion angle in closed (blue) and open (green) forms.

functionalized SAMs consists in designing rigid molecules with geometry constrained to their highest hyperpolarizability conformation.

4 Conclusions

In this work, we have used a sequential multiscale approach combining atomistic MD simulations and DFT calculations to evaluate the second harmonic generation responses of photoresponsive SAMs based on indolino-oxazolidine derivatives. MD simulations revealed that photoresponsive regions of the SAMs exhibit a high degree of orientational and positional disorder due to the flexibility of the photoresponsive units (in particular that of the thioalkyl group), which on the one hand is detrimental for crystalline packing, and on the other hand makes the chromophore conformation highly sensitive to intermolecular interactions. Quite interestingly, DFT calculations carried out on a large selection of simulated molecular structures evidence that, despite large geometrical distortions of the photochromic molecules and the lack of orientational order, IND-based SAMs are expected to display a good contrast in first hyperpolarizability upon the photochromic conversion, of the same order of magnitude as that observed in the isolated molecule.

As already known from previous studies,[16] the large NLO enhancement from the closed to the open configuration can be attributed to the increase of the π-electron conjugation between the indolino-oxazolidine and bithiophene moieties, as described by the strong decrease of the bond length alternation along the vinyl linker connecting these two units. More surprising was the correlation found between the magnitude of the first hyperpolarizability in both forms and the torsional angle γ around the single bond between bithiophene and thioalkyl groups. Since this rotation is quasi barrierless in the isolated molecule, the statistical distribution of this dihedral angle is very broad for both forms of the SAMs studied here. In such a case, only controlling by chemical design the shape of this distribution in newly synthesized indolino-oxazolidine derivatives would allow maximizing their NLO responses. More generally, these results tell us that calculations of the NLO properties of isolated molecules allows a reliable screening of the most effective compounds for subsequent integration in 2D materials, but also highlight that optimizing the NLO responses of devices requires a fine control of the intermolecular interactions, which induce significant distortions in the molecular structure. Reducing the flexibility of the photoresponsive molecular units, together with variations of the coverage rate or the use of bulky separators, appear as promising strategies.

Mutual polarization effects and intermolecular couplings, not considered in this first study, might also impact the NLO responses of the SAMs. Future investigations, carried out on a representative set of molecular aggregates, are expected to provide design rules to effectively exploit the collective effects for optimizing the amplitude of the NLO responses of the system, as well as their contrast upon commutation. The sequential MD-QM approach implemented here promises to be a highly useful computational tool to explore these different alternatives.

Finally, since the MD simulations were conducted on SAMs with fully closed or open forms, assuming therefore the switching of 100% of the chromophores, it would also be interesting to investigate the light-induced dynamic effects. These investigations should provide key information on the switching efficiency in these densely packed systems.

Conflicts of interest

There are no conflicts to declare.

Acknowledgements

K. P. thanks the Région Aquitaine (INMERON Project, convention 2014-1R10102-00002867) and the University of Namur for co-financing her PhD grant. This work was carried out in the frame of the Centre of Excellence LAPHIA (Investments for the future: Programme IdEx Bordeaux – LAPHIA (ANR-10-IDEX-03-02). It was also supported by funds from the M-ERA.NET project MODIGLIANI (ANR-15-MERA-0002-01) and from the Francqui Foundation. The calculations were performed on the computing facilities of the Consortium des Equipements de Calcul Intensif (CECI, http://www.ceci-hpc.be), and particularly those of the Technological Platform on High-Performance Computing, for which we gratefully acknowledge the financial support of the FNRS-FRFC (Conventions No. 2.4.617.07.F and 2.5020.11) and of the University of Namur, on Zenobe, the Tier-1 facility of the Walloon Region (Convention 1117545), as well as on the Mésocentre de Calcul Intensif Aquitain (MCIA) of the University of Bordeaux, financed by the Conseil Régional d'Aquitaine and the French Ministry of Research and Technology. L.M, B.C. and F.C thank Prof. Vincent Rodriguez for helpful discussions.

Notes and references

1 *Molecular Switches, Second Edition*, ed. W. R. Feringa, B. L.; Browne, Wiley-VCH, Weinheim, 2011.
2 E. Orgiu and P. Samorì, *Adv. Mater.*, 2014, **26**, 1827–1845.
3 J. Andréasson and U. Pischel, *Chem. Soc. Rev.*, 2015, **44**, 1053–1069.
4 W. R. Browne and B. L. Feringa, *Annu. Rev. Phys. Chem.*, 2009, **60**, 407–428.
5 S. Casalini, C. A. Bortolotti, F. Leonardi and F. Biscarini, *Chem. Soc. Rev.*, 2017, **46**, 40–71.
6 T. Lummerstorfer and H. Hoffmann, *J. Phys. Chem. B*, 2004, **108**, 3963–3966.
7 C. Haensch, S. Hoeppener and U. S. Schubert, *Chem. Soc. Rev.*, 2010, **39**, 2323–2334.
8 C. Nicosia and J. Huskens, *Mater. Horiz.*, 2014, **1**, 32–45.
9 B. J. Coe, *Chem. Eur. J.*, 1999, **5**, 2464–2471.
10 I. Asselberghs, K. Clays, A. Persoons, M. D. Ward and J. McCleverty, *J. Mater. Chem.*, 2004, **14**, 2831–2839.
11 F. Castet, V. Rodriguez, J.-L. Pozzo, L. Ducasse, A. Plaquet and B. Champagne, *Acc. Chem. Res.*, 2013, **46**, 2656–2665.
12 M. Schulze, M. Utecht, T. Moldt, D. Przyrembel, C. Gahl, M. Weinelt, P. Saalfrank and P. Tegeder, *Phys. Chem. Chem. Phys.*, 2015, **17**, 18079–18086.
13 M. Schulze, M. Utecht, A. Hebert, K. Rück-Braun, P. Saalfrank and P. Tegeder, *J. Phys. Chem. Lett.*, 2015, **6**, 505–509.

14 L. Sanguinet, J. L. Pozzo, V. Rodriguez, F. Adamietz, F. Castet, L. Ducasse and B. Champagne, *J. Phys. Chem. B*, 2005, **109**, 11139–11150.

15 F. Mançois, J.-L. Pozzo, J. Pan, F. Adamietz, V. Rodriguez, L. Ducasse, F. Castet, A. Plaquet and B. Champagne, *Chem.–Eur. J.*, 2009, **15**, 2560–2571.

16 K. Pielak, F. Bondu, L. Sanguinet, V. Rodriguez, B. Champagne and F. Castet, *J. Phys. Chem. C*, 2017, **121**, 1851–1860.

17 J. Wang, R. M. Wolf, J. W. Caldwell, P. A. Kollman and D. A. Case, *J. Comput. Chem.*, 2004, **25**, 1157–1174.

18 A. Pizzirusso, M. E. D. Pietro, G. D. Luca, G. Celebre, M. Longeri, L. Muccioli and C. Zannoni, *ChemPhysChem*, 2014, **15**, 1356–1367.

19 Y. Zhao and D. G. Truhlar, *Theor. Chem. Acc.*, 2008, **120**, 215–241.

20 M. de Wergifosse and B. Champagne, *J. Chem. Phys.*, 2011, **134**, 074113.

21 L. E. Johnson, L. R. Dalton and B. H. Robinson, *Acc. Chem. Res.*, 2014, **47**, 3258–3265.

22 K. Garrett, X. Sosa Vazquez, S. B. Egri, J. Wilmer, L. E. Johnson, B. H. Robinson and C. M. Isborn, *J. Chem. Theory Comput.*, 2014, **10**, 3821–3831.

23 M. J. Frisch, G. W. Trucks, H. B. Schlegel, G. E. Scuseria, M. A. Robb, J. R. Cheeseman, G. Scalmani, V. Barone, B. Mennucci, G. A. Petersson, H. Nakatsuji, M. Caricato, X. Li, H. P. Hratchian, A. F. Izmaylov, J. Bloino, G. Zheng, J. L. Sonnenberg, M. Hada, M. Ehara, K. Toyota, R. Fukuda, J. Hasegawa, M. Ishida, T. Nakajima, Y. Honda, O. Kitao, H. Nakai, T. Vreven, J. A. Montgomery, Jr., J. E. Peralta, F. Ogliaro, M. Bearpark, J. J. Heyd, E. Brothers, K. N. Kudin, V. N. Staroverov, R. Kobayashi, J. Normand, K. Raghavachari, A. Rendell, J. C. Burant, S. S. Iyengar, J. Tomasi, M. Cossi, N. Rega, J. M. Millam, M. Klene, J. E. Knox, J. B. Cross, V. Bakken, C. Adamo, J. Jaramillo, R. Gomperts, R. E. Stratmann, O. Yazyev, A. J. Austin, R. Cammi, C. Pomelli, J. W. Ochterski, R. L. Martin, K. Morokuma, V. G. Zakrzewski, G. A. Voth, P. Salvador, J. J. Dannenberg, S. Dapprich, A. D. Daniels, Farkas, J. B. Foresman, J. V. Ortiz, J. Cioslowski and D. J. Fox, *Gaussian 09 revision D01*, Gaussian Inc. Wallingford CT 2009.

24 A. Willetts, J. E. Rice, D. M. Burland and D. P. Shelton, *J. Chem. Phys.*, 1992, **97**, 7590–7599.

25 H. Reis, *J. Chem. Phys.*, 2006, **125**, 014506.

26 O. M. Roscioni, L. Muccioli, A. Mityashin, J. Cornil and C. Zannoni, *J. Phys. Chem. C*, 2016, **120**, 14652–14662.

27 S. Nénon and B. Champagne, *J. Chem. Phys.*, 2013, **138**, 204107.

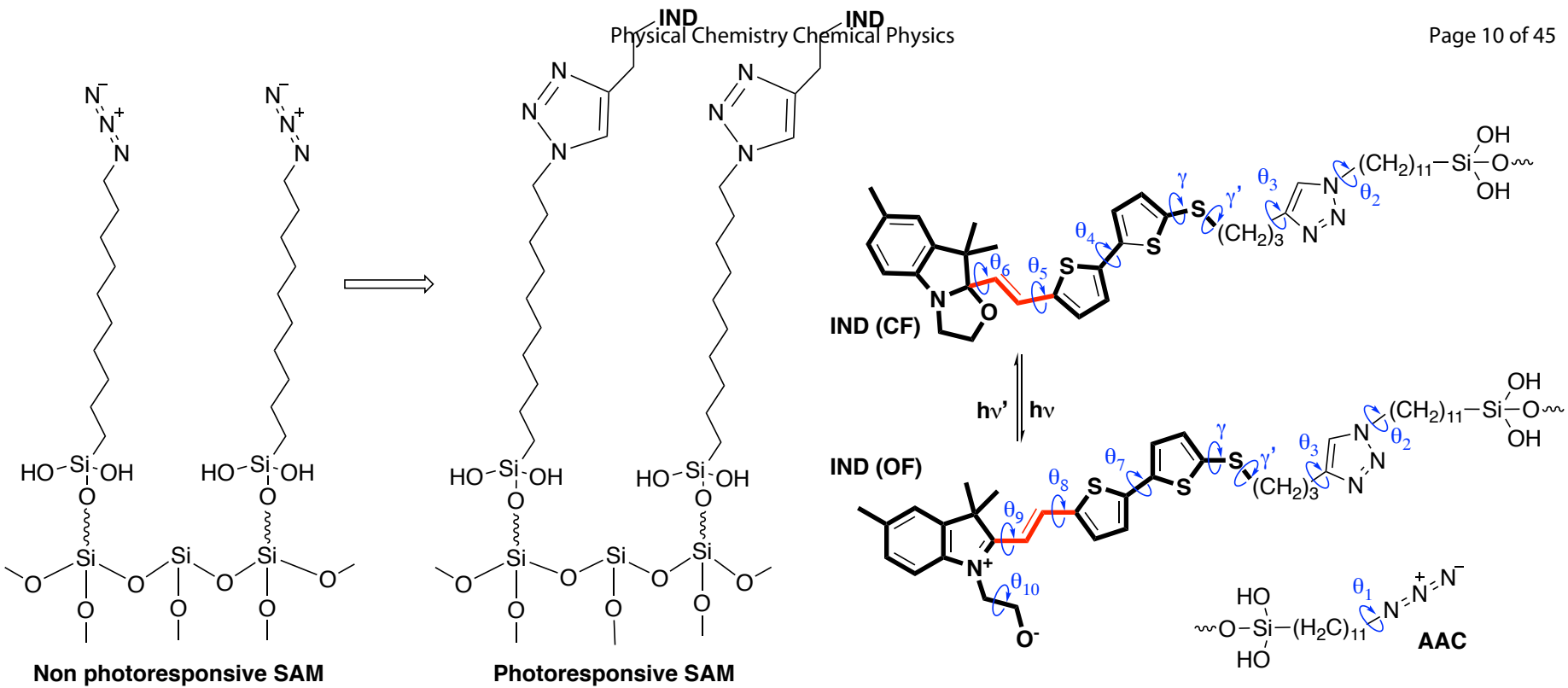
IND
IND
Non photoresponsive SAM
Photoresponsive SAM
IND (CF)
hν'
hν
IND (OF)
AAC

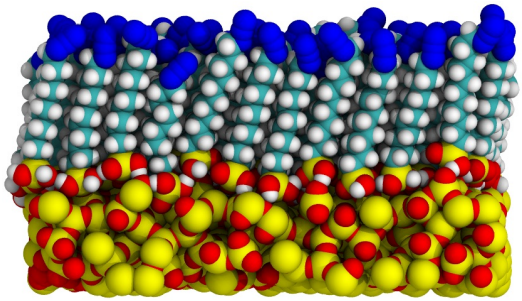

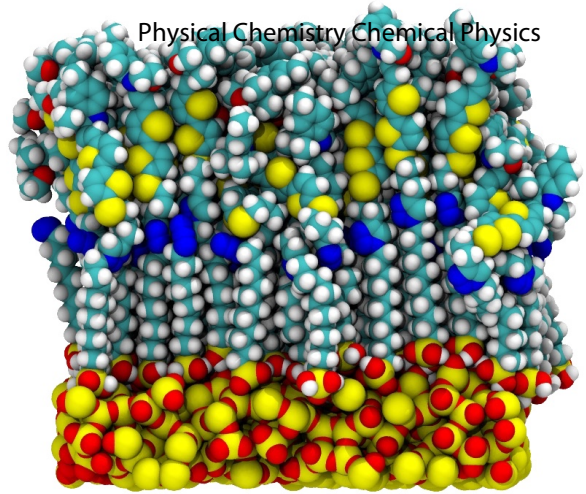

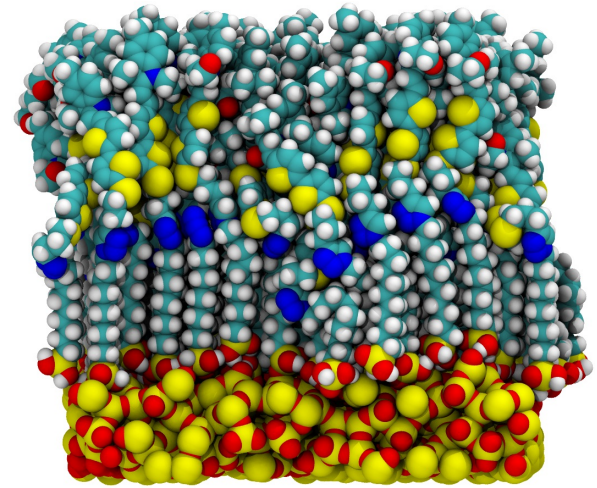

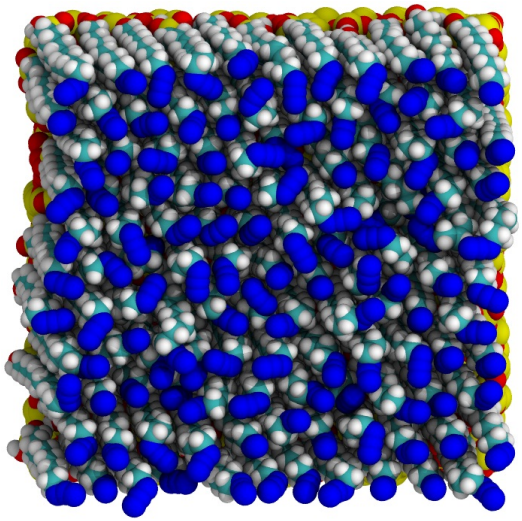

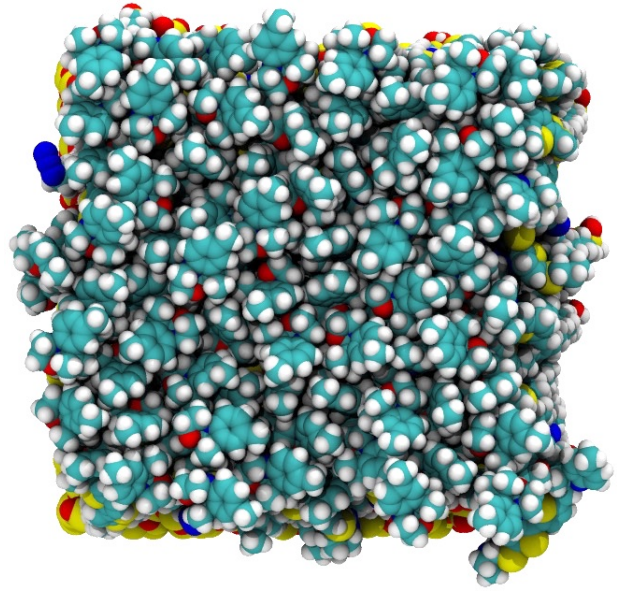

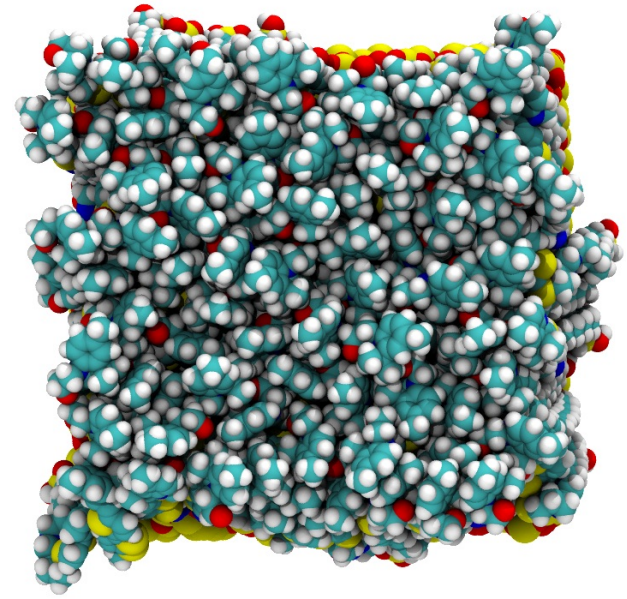

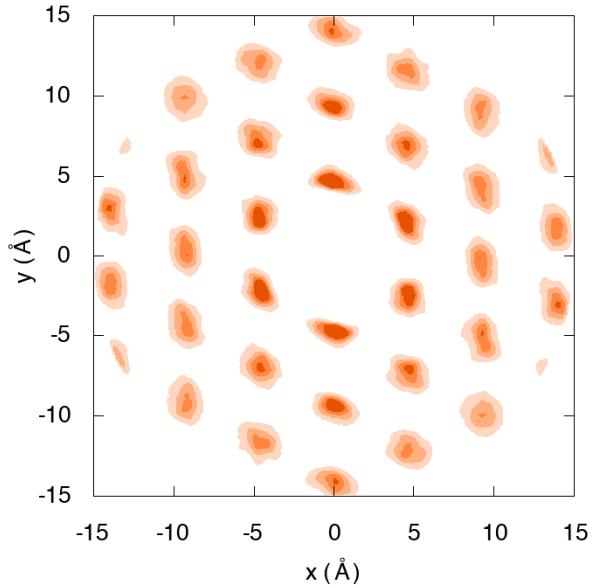
15
10
5
0
-5
-10
-15
y (Å)
-15 -10 -5 0 5 10 15
x (Å)

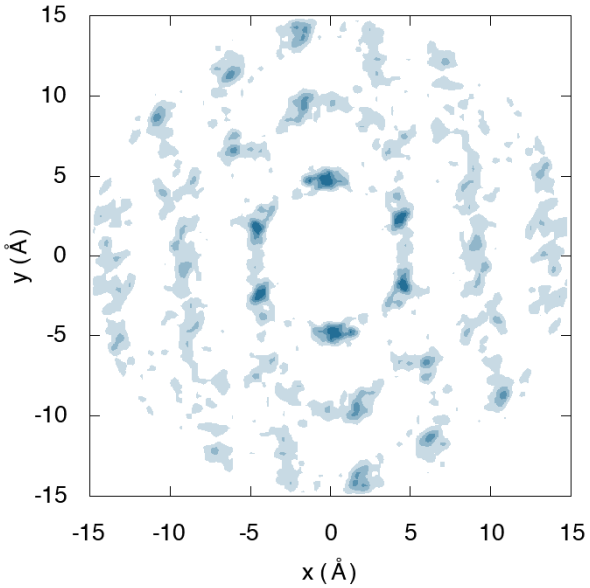
15
10
5
0
-5
-10
-15
y (Å)
-15 -10 -5 0 5 10 15
x (Å)

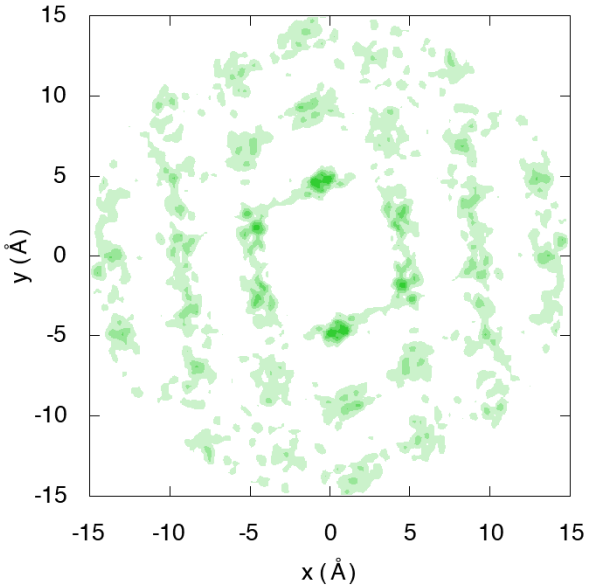
15
10
5
0
-5
-10
-15
y (Å)
-15 -10 -5 0 5 10 15
x (Å)

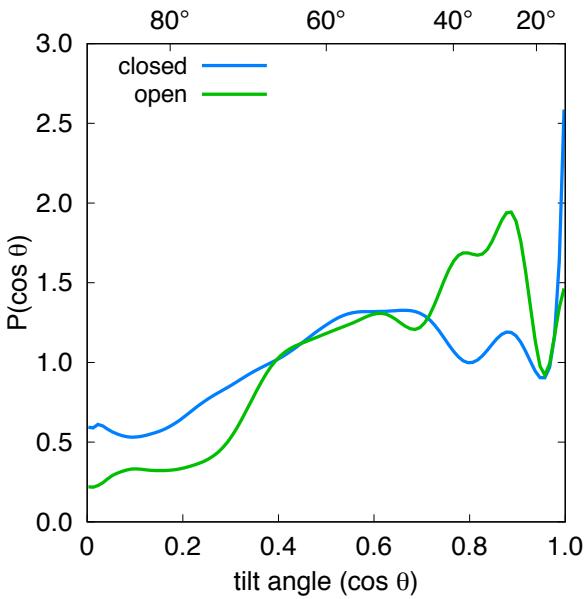
80°
60°
40°
20°
closed
open
3.0
2.5
2.0
1.5
1.0
0.5
0.0
P(cos θ)
0 0.2 0.4 0.6 0.8 1.0
tilt angle (cos θ)

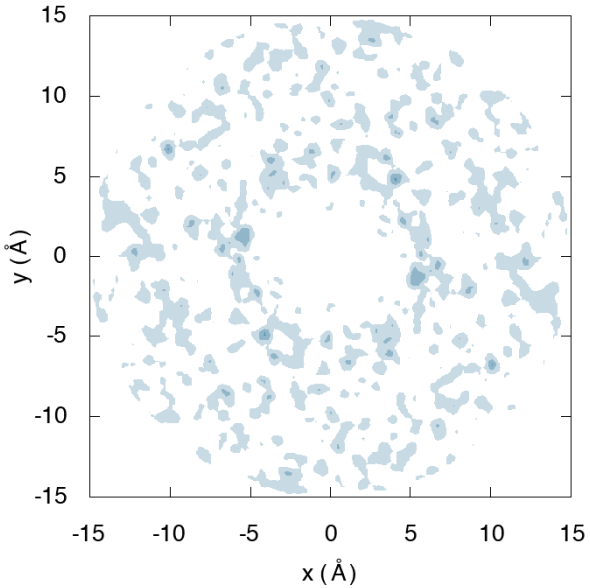
15
10
5
0
-5
-10
-15
y (Å)
-15 -10 -5 0 5 10 15
x (Å)

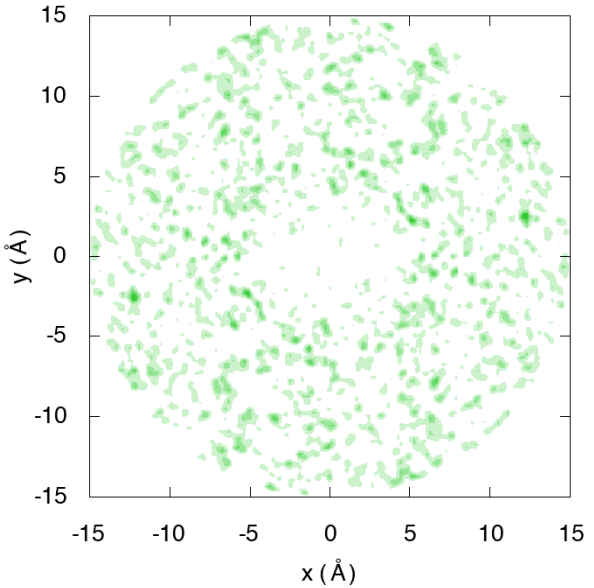
15
10
5
0
-5
-10
-15
y (Å)
-15 -10 -5 0 5 10 15
x (Å)

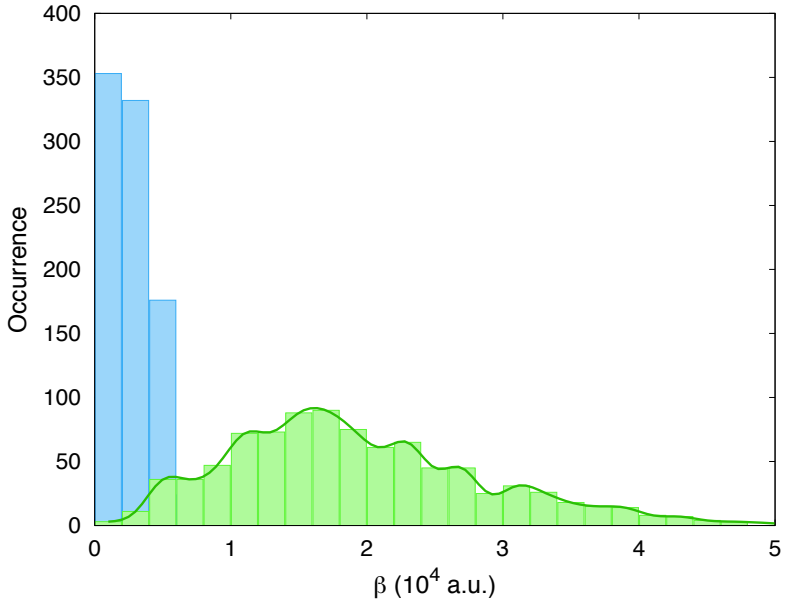
Occurrence
β (10^4 a.u.)

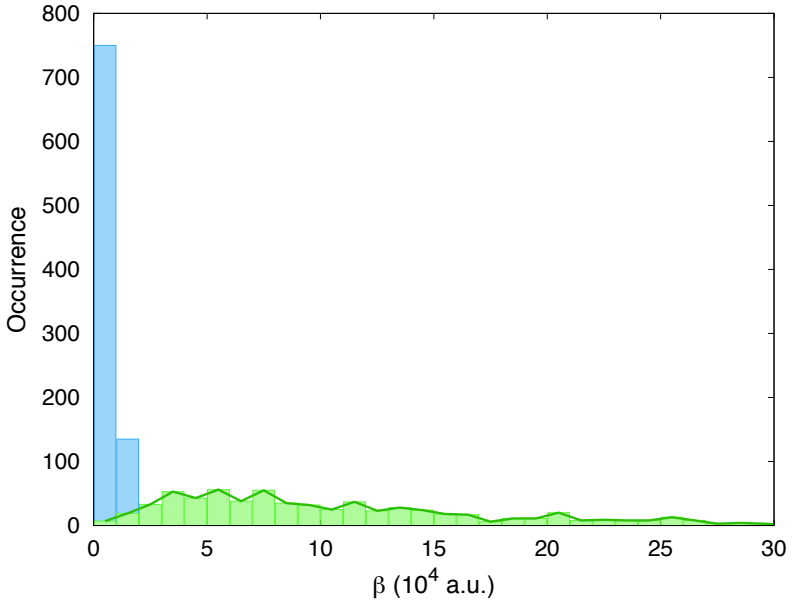
Occurrence
β (10^4 a.u.)

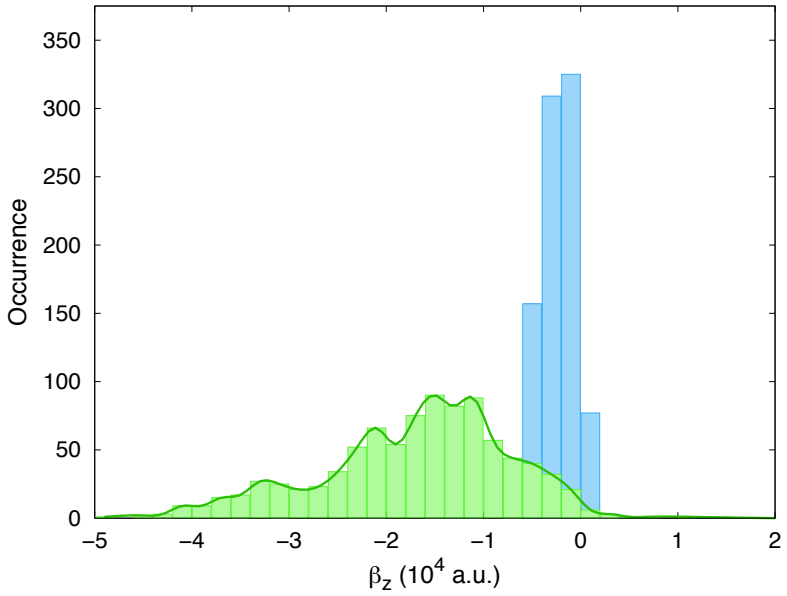
Occurrence
β_z (10^4 a.u.)

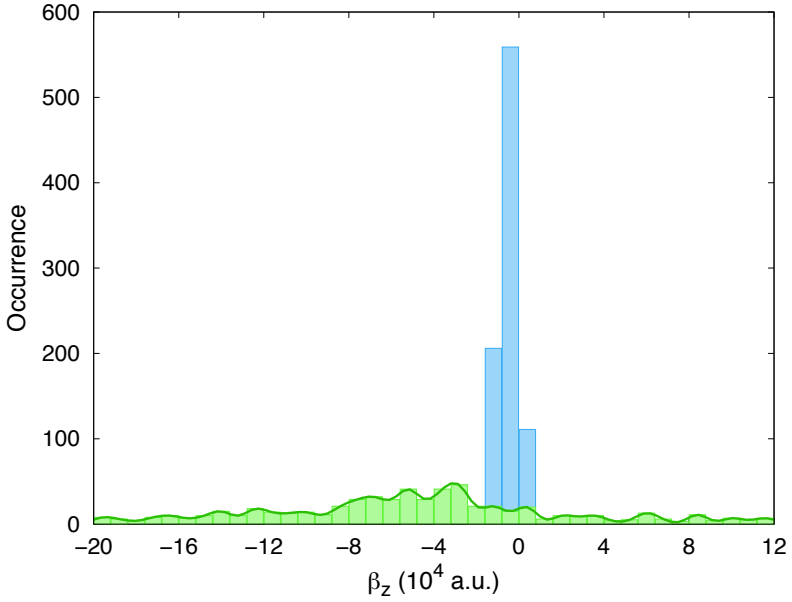
Occurrence
β_z (10^4 a.u.)

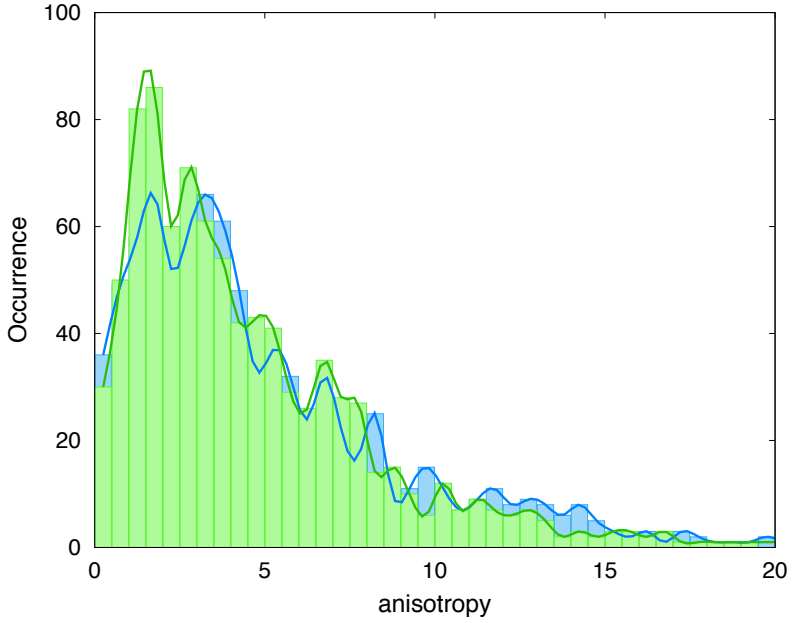
Occurrence
anisotropy

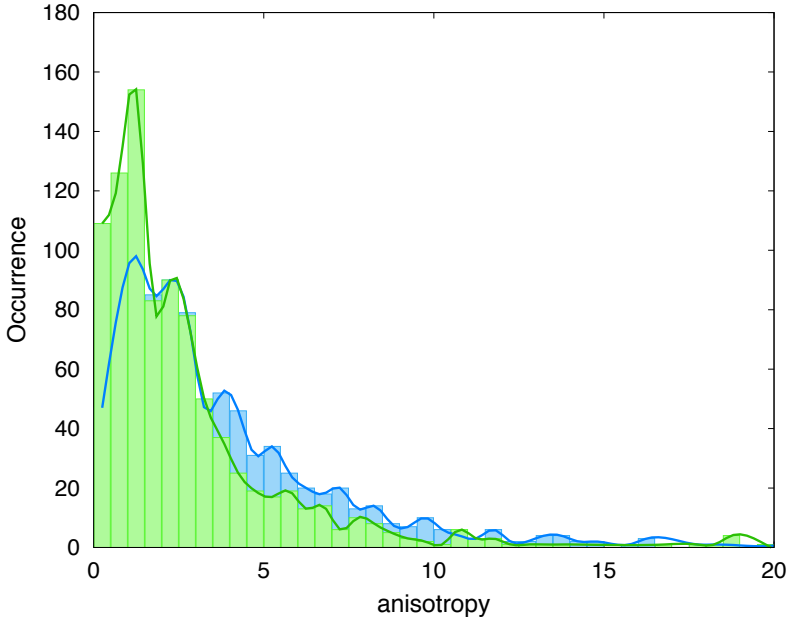
Occurrence
anisotropy

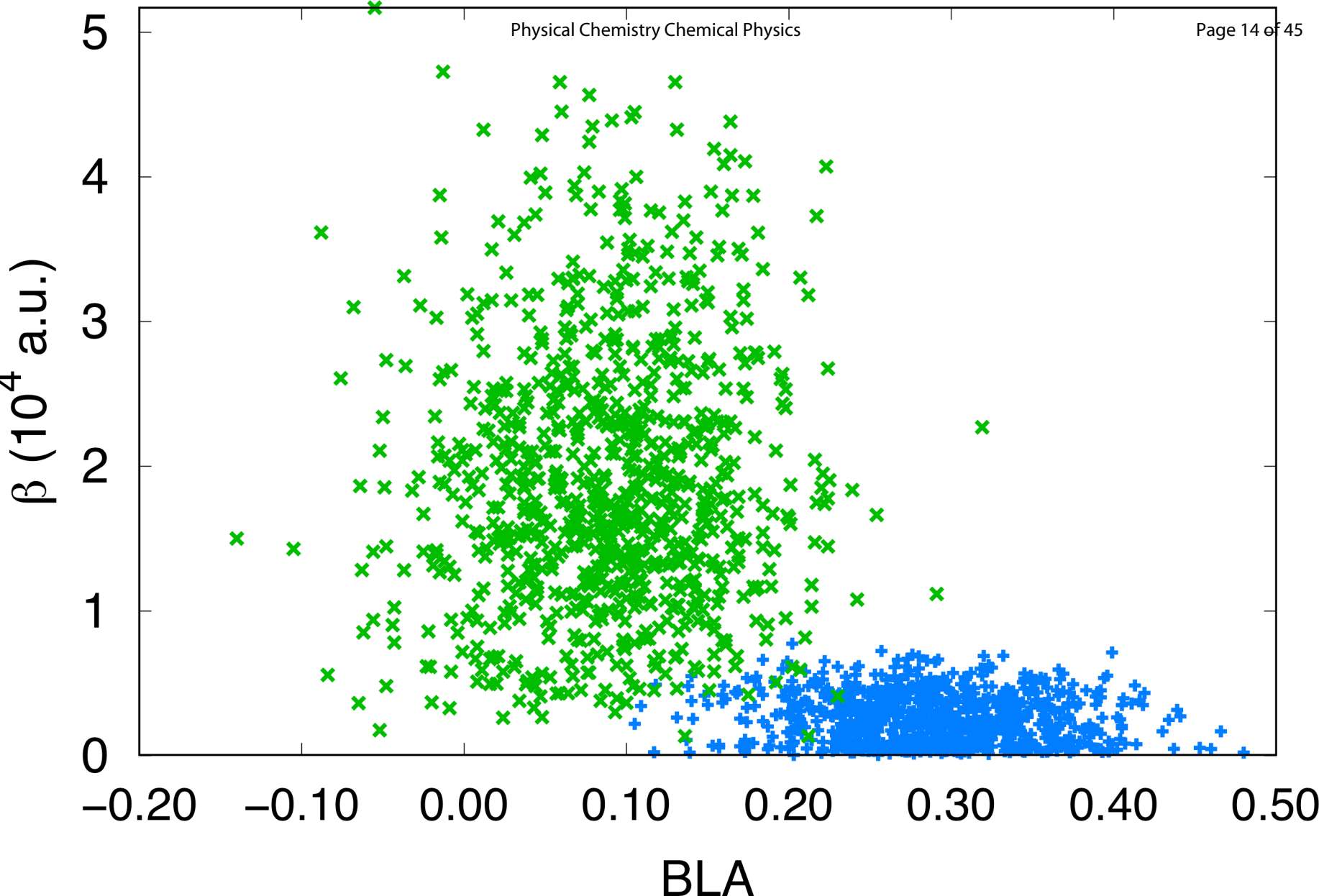
β (10^4 a.u.)
5
4
3
2
1
0
–0.20
–0.10
0.00
0.10
0.20
0.30
0.40
0.50
BLA

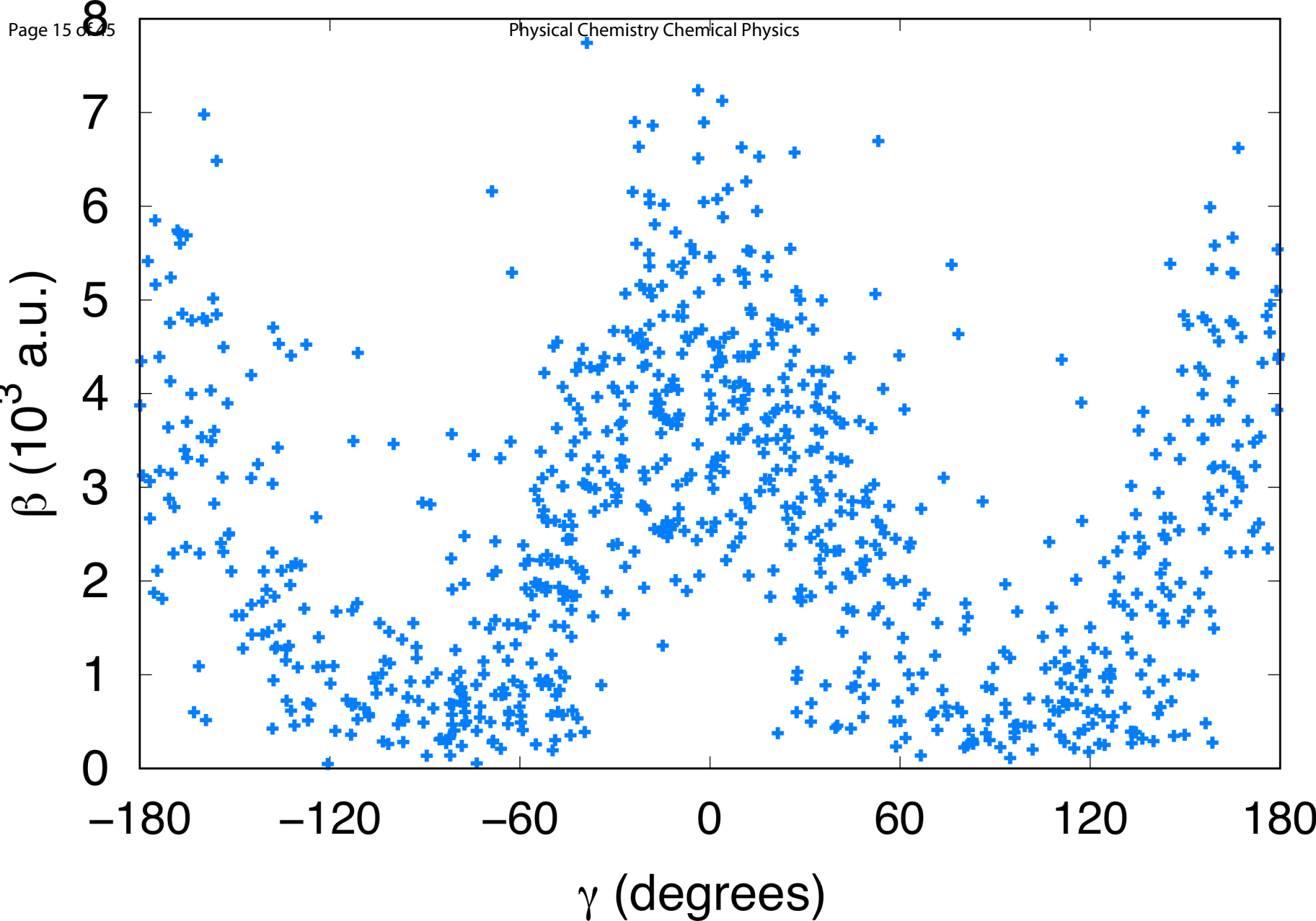
β (10^3 a.u.)
γ (degrees)
0
1
2
3
4
5
6
7
8
−180
−120
−60
0
60
120
180

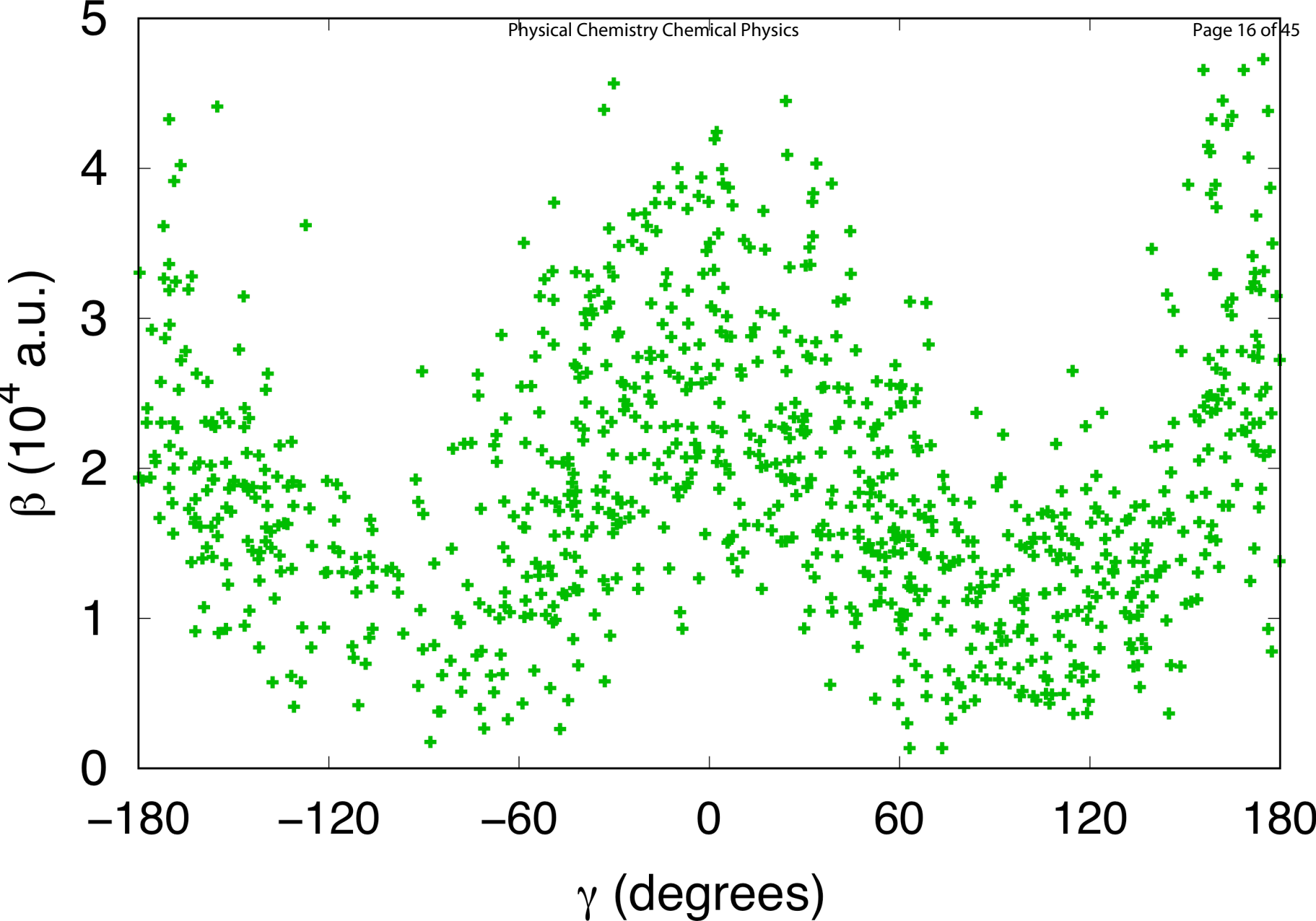
β (10^4 a.u.)
5
4
3
2
1
0
−180
−120
−60
0
60
120
180
γ (degrees)

Supporting information for: Nonlinear Optical Responses Of Self-Assembled Monolayers Functionalized With Indolino-Oxazolidine Photoswitches

Claire Tonnelé,[*,†] Kornelia Pielak,[‡,¶] Jean Deviers,[‡] Luca Muccioli,[§] Benoit Champagne,[*,¶] and Frédéric Castet[*,‡]

†*Institut des Sciences Moléculaires (ISM, UMR CNRS 5255), University of Bordeaux, 351 Cours de la Libération, 33405 Talence, France*

‡*Institut des Sciences Moléculaires (ISM, UMR CNRS 5255), University of Bordeaux, 351 Cours de la Libération, 33405 Talence, France*

¶*Unité de Chimie Physique Théorique et Structurale, Chemistry Department, Namur Institute of Structured Matter, University of Namur, Belgium*

§*Department of Industrial Chemistry "Toso Montanari", University of Bologna, Viale Risorgimento 4, 40136 Bologna, Italy*

E-mail: claire.tonnele@u-bordeaux.fr; benoit.champagne@unamur.be; frederic.castet@u-bordeaux.fr

Force field parameterization

Torsional potentials around the $\theta_1 - \theta_{10}$ dihedrals (Figure SI-1) were derived from DFT calculations performed at the M06/6-311G(d) level. The DFT and re-parameterized molecular mechanics torsional potentials are displayed in Figure SI-2.

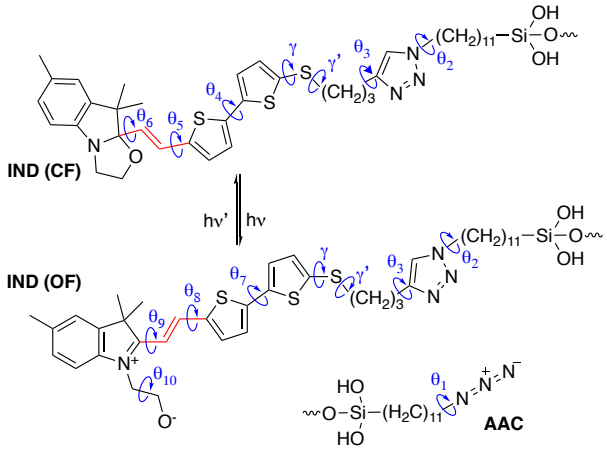

Figure SI-1: Scheme of the photochromic switchable closed form (CF) and open form (OF) of the indolino-oxazolidine (IND) derivative, and azido-undecylsilane chain (AAC). Force field parameters have been re-calculated for torsions θ_1 to θ_{10}. The dihedrals are defined as follows: θ_1 =NNCC, θ_2 =CCNC, θ_3 =NCCC, θ_4 =SCCS, θ_5 =SCCC, θ_6 =CCCN, θ_7 =SCCS, θ_8 =SCCC, θ_9 =CCCN, θ_{10} =NCCO, γ =CSCC, γ' =CSCC.

Preparation of the SiO_2 surface

Simulations were carried out using Clay force field[S1] to describe amorphous silica. A bulk sample was prepared following a procedure similar to the one reported by Della Valle *et al.*[S2] and described hereafter. A box of dimensions $52.044 \times 51.119 \times 30.000$ Å^3 was filled with 1745 Si atoms and 3490 O atoms randomly distributed (using Packmol[S3]) to achieve the experimental density[S4] of vitreous silica at room temperature (2.2 g·cm^{-3}). An energy minimization was performed to avoid possible steric clashes or irregularities in the input structure, applying 3D periodic boundary conditions. The sample was then heated up to 4000 K (i) for the first 100 ps, a 0.2 fs timestep was used and velocities rescaled every step,

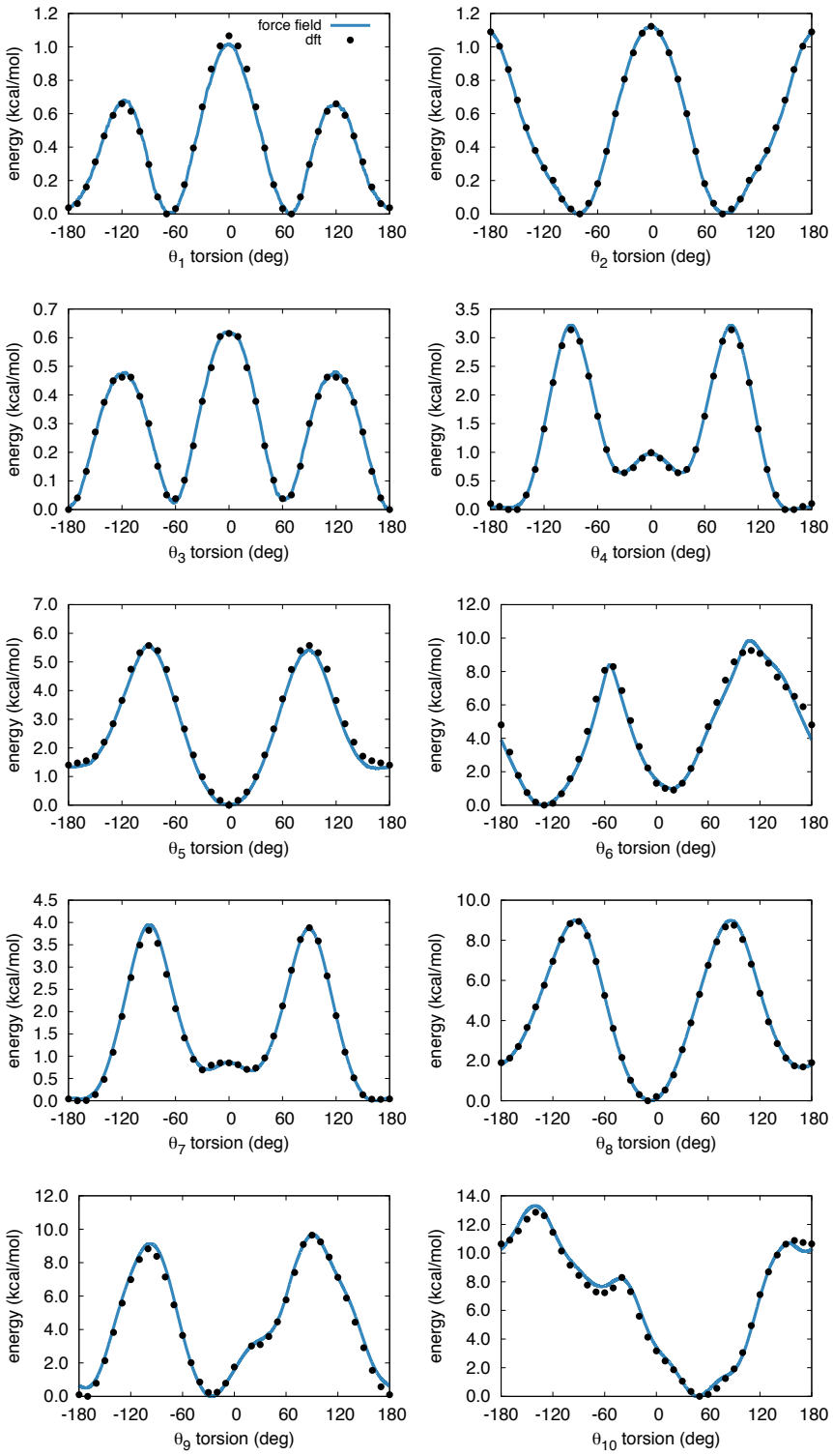

Figure SI-2: DFT and re-parameterized molecular mechanics torsional potentials around dihedrals $\theta_1 - \theta_{10}$ (see Scheme SI-1).

(ii) for additional 80 ps, time step was increased to 0.4 fs and put in contact with a heat bath simulated using Lowe-Andersen thermostat with a collision rate of 1 fs^{-1}. To obtain an amorphous silica glass, the sample was subsequently gradually cooled down to 300 K at a rate of 0.01 K/0.5 fs for 185 ps and equilibrated for additional 100 ps at 300 K. A 10 ns equilibration was performed before a production run of 1 ns for subsequent characterization of the amorphous sample.

The pair radial distribution functions $g_{ij}(r)$ were computed and are in close agreement with the X-Ray diffraction measurements (in orange) from Mozzi *et al.*[S4], as shown in Figure SI-3. From the integral to the first minimum of $g_{ij}(r)$ one can determine a coordination number of 3.93 and 1.96 for the Si and O atoms, respectively (expected 4 and 2, respectively). A

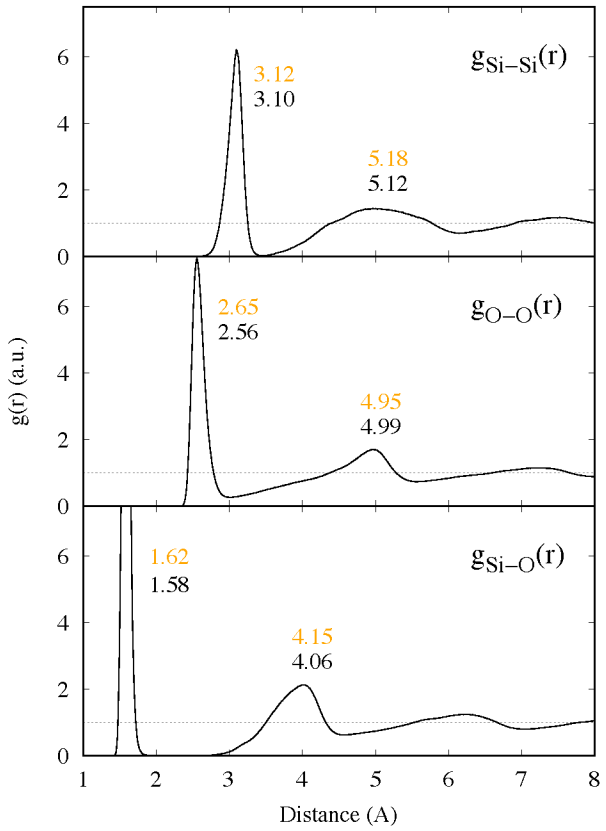

Figure SI-3: Radial distribution functions $g(r)$ for Si–Si pairs (top), O-O pairs (middle) and Si-O pairs (bottom), computed at 300 K for amorphous silica. Experimental (orange) distances[S4] are shown for each peak together with theoretical values (black).

glass surface was then obtained using an approach similar to that described by Feuston and

Garofalini[S5]. The simulation box was extended to 150 Å in the z direction, rendering the periodic boundary conditions effective only in the x and y directions for the resulting SiO_2 slab and a 20 Å-thick layer of atoms was kept immobile at the bottom (Figure SI-4). The free surface was annealed at 1000 K for 1 ns to mimic the spontaneous heating during the fracture, as well as to help the local surface reconstruction and structure relaxation. The sample was then gradually cooled down to 300 K at a rate of 0.02 K/fs and further relaxed for 5 ns. Based on the assumption that the grafted molecules link to the surface via a Si-

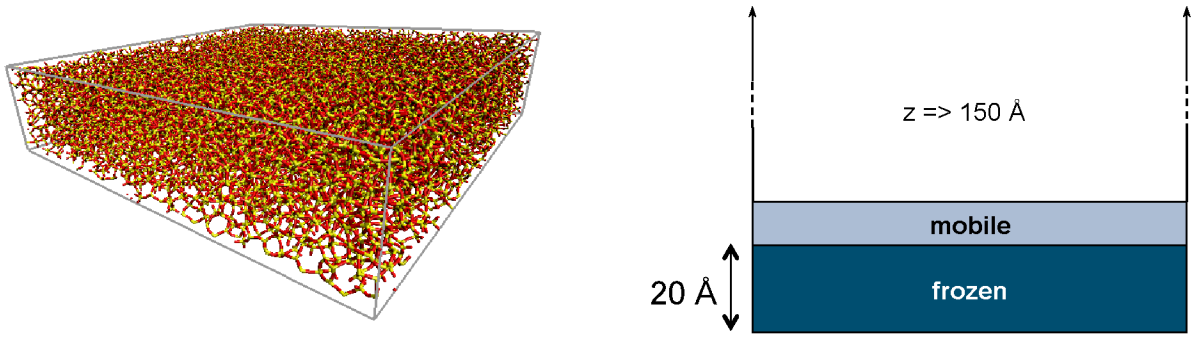

Figure SI-4: Equilibrated bulk of amorphous SiO_2 (left), and sketch of the simulation box used for the SiO_2 surface (right).

O single bond, one hydroxyl hydrogen of the -Si-$(OH)_3$ group was removed and its charge summed to the one of the corresponding oxygen atom. The surface was prepared for grafting as follows: oxygen atoms with coordination number of 1 located at $z > 27$ Å were removed from the slab and the corresponding total charge redistributed over the atoms of the frozen layer ($z \leq 20$ Å). A specific Lennard-Jones interaction ($\epsilon = -0.1554$ kcal/mol, $r = 1.64$ Å) was then added between alkylsilane grafting oxygens and "reactive" silicon atoms from the surface (the ones previously bonded to monocoordinate oxygen atoms), providing an effective bond without explicit grafting.[S6]

Functionalized surfaces with various coverage rates

After the preparation of a fully covered azidoalkyl SAM, only a fraction of the azide groups was substituted by chromophore units, with the rationale of avoiding a too close packing of the chromophores onto the surface that could hamper the efficiency of the switching process. Three samples with different relative chromophore fraction (1/4, 1/2 and 3/4) were generated, corresponding to coverages of 1.13, 2.26 and 3.38 molecules/nm^2, respectively. As can be seen in Figure SI-5, decreasing the coverage induces a decrease of the SAM thickness, evaluated as the average difference between the height of the complete system and that of the SiO_2 surface alone. The numerical data are collected in Table SI-1.

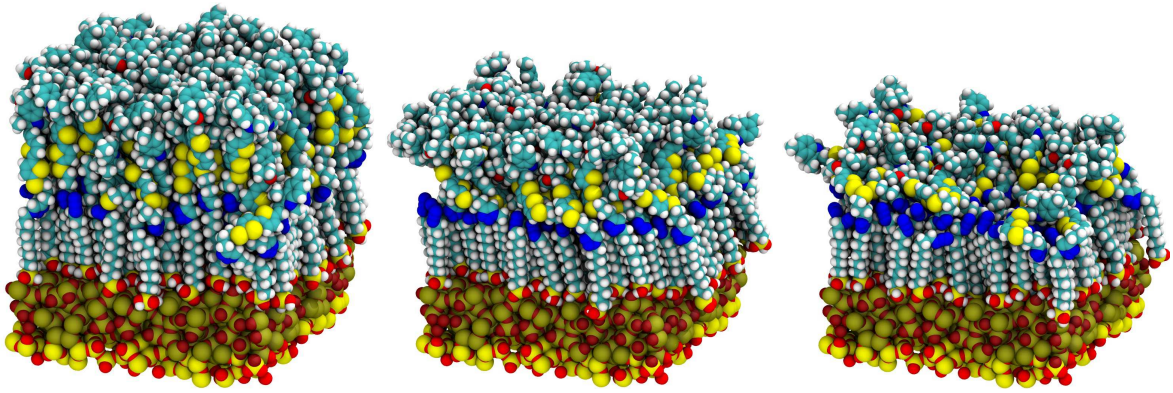

Figure SI-5: From left to right: SAMs functionalized with the closed IND molecule, with relative grafting ratios of 1/4, 1/2 and 3/4.

Table SI-1: Average value of the cosine of the tilt angle, θ_{tilt}), defined as the angle between the double C-C bond of the vinyl bridge (red segment in Fig. SI-1) and the axis normal to the surface plane. Thickness and roughness (both in Å) of the SAM in its closed form (CF) and in its open form (OF), with respect to the relative coverage (1/4, 1/2 or 3/4).

Property	CF (1/4)	CF (1/2)	CF (3/4)	OF (3/4)
$\cos^2(\theta_{tilt})$	0.220	0.396	0.362	0.448
Thickness	26.68	33.96	40.40	40.56
Roughness	3.15	2.03	1.32	1.44

Choice of the relevant molecular fragment for NLO calculations

Before running NLO calculations on molecular structures extracted from MD simulations, preliminary tests were carried out to define the size of the fragments that should be considered. The complete reference molecule (IND1 in Figure SI-6), including from the indolino-oxazolidine photoresponsive part to the terminal $Si(OH)_3$ anchoring unit was first optimized at the M06/6-311G(d) level, and its first hyperpolarizability β subsequently calculated at the M06-2X/6-311G(d) level. Then, the NLO properties of the simplified fragments illustrated in Figure SI-6 were calculated at the same level of theory, without performing any further geometrical relaxation. So, in the IND2 fragment, the $Si(OH)_3$ anchor was removed and replaced by an hydrogen atom; starting from IND2, the alkyl chain was removed in IND3 and replaced by a simple methyl group; finally, the triazole moiety as well as the central $(CH_2)_3$ chain were removed and replaced by a methyl group in IND4. The geometries of the refer-

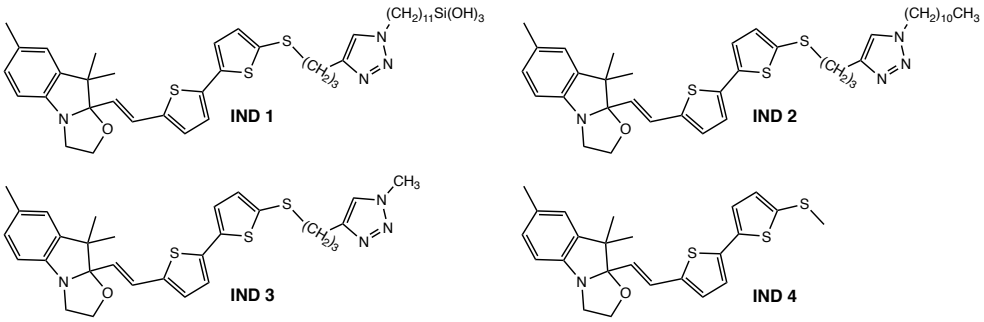

Figure SI-6: Molecular fragments considered in DFT calculations of the NLO properties.

ence open and closed conformers are illustrated in Figure SI-7, and the relevant geometrical parameters are gathered in Table SI-2. The β values calculated for the four IND 1-4 systems in both their closed and open forms are collected in Table SI-3. According to a previous study on indolino-oxazolidine molecules in solution (corresponding to the IND4 system),[S7] one single conformer exists at room temperature for the closed form, while three conformers differing by the values of the θ_7 and θ_9 dihedrals exhibit non negligible populations for the open form. The corresponding three conformers were therefore considered as starting struc-

tures for geometry optimizations of the OF in the present study. The static and dynamic

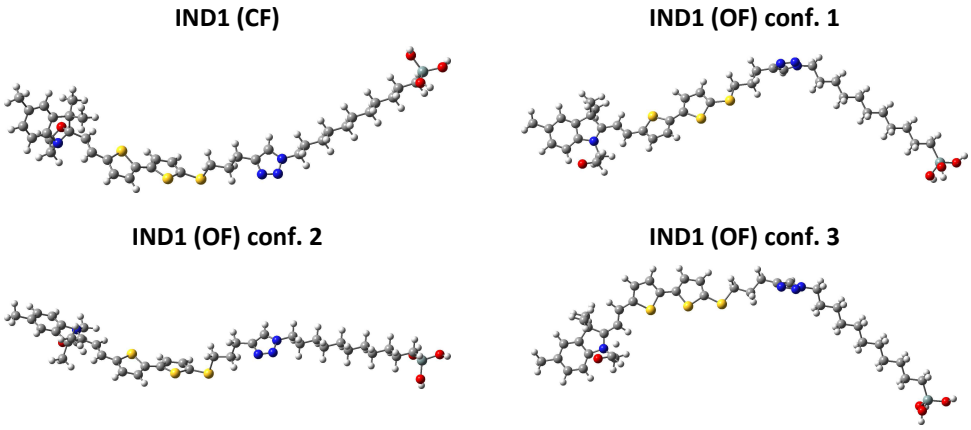

Figure SI-7: Geometry of the reference IND1 molecules optimized at the M06/6-311G(d) level.

hyperpolarizabilities of the closed form (CF) and open form (OF) of the four systems defined in Figure SI-6 are collected in Table SI-3, while the $\beta(OF)/\beta(CF)$ contrast ratios are reported in Table SI-4. The results lead to similar conclusions for the static and dynamic cases. With the exception of the relatively large ∼10% error obtained for the dynamic β of the conformer 3 (IND2 OF), removing the terminal $Si(OH)_3$ anchoring unit neither impacts the β values, which deviate from the reference ones by $< 4\%$ for the CF and $< 1\%$ for the OF, nor the OF/CF contrasts, for which the errors are smaller than 5%. Removing the alkyl chain induces slightly larger errors on the β values of both CF and OF, but the latter remain lower than 10%, again with the exception of the dynamic value of conformer 3 (IND3 OF), which reaches 22%. Finally, the most simplified IND4 system leads to large errors on β, of the order of 60% for the CF and ranging from 22% to 47% for OF; in addition OF/CF contrasts are significantly overestimated. On the basis of these results, the IND2 fragment was selected as the best trade-off between accuracy and calculation time for all further DFT calculations of the NLO properties of the photochromic molecules extracted from the MD simulation trajectory.

Table SI-2: Bond Length Alternation (BLA, Å) along the vinyl bridge of the indolino-oxazolidine moiety (red segment in Fig. SI-1, and torsional angles (θ_{5-9} and γ, degrees) calculated at the M06/6-311G(d) level for the reference system (IND1) defined in Figure SI-6 in its closed and open form (CF, OF). Three different conformers are considered for the OF.

System (form)	Conf.	BLA	θ_4	θ_5	θ_6	γ
IND1 (CF)	1	-0.135	158.1	1.2	-17.7	101.7
System (form)	Conf.	BLA	θ_7	θ_8	θ_9	γ
IND1 (OF)	1	-0.051	-167.1	-5.9	-24.9	-16.4
IND1 (OF)	2	-0.055	158.5	2.5	-174.6	99.8
IND1 (OF)	3	-0.053	-25.8	3.3	-173.2	7.1

Table SI-3: Static ($\lambda = \infty$) and dynamic ($\lambda = 1064$ nm) hyperpolarizabilities (β, a.u.) calculated at the M06-2X/6-311G(d) level for the four systems defined in Figure SI-6 in their closed and open form. Three conformers (Conf.) are considered for the open forms. The relative differences (% Diff.) between the β values calculated for the IND2-4 systems and the reference IND1 system are also reported. All β values are given in atomic units (1 au of $\beta = 3.6310^{-42}$ $\mathbf{m}^4\mathbf{V}^{-1} = 3.2063 \times 10^{-53}$ $\mathbf{C}^3\mathbf{m}^3\mathbf{J}^{-2} = 8.641 \times 10^{-33}$ esu).

		$\lambda = \infty$		$\lambda = 1064$ nm	
System (form)	Conf.	β	% Diff.	β	% Diff.
IND1 (CF)	1	846	/	1306	/
IND2 (CF)	1	878	3.66	1325	1.45
IND3 (CF)	1	797	-5.90	1193	-8.65
IND4 (CF)	1	334	-60.57	468	-64.17
System (form)	Conf.	β	% Diff.	β	% Diff.
IND1 (OF)	1	13668	/	114016	/
IND2 (OF)	1	13572	-0.70	113328	-0.60
IND3 (OF)	1	12766	-6.60	109830	-3.67
IND4 (OF)	1	8967	-34.39	89040	-21.91
IND1 (OF)	2	3961	/	27787	/
IND2 (OF)	2	3965	0.10	25094	-9.69
IND3 (OF)	2	3941	-0.50	21669	-22.02
IND4 (OF)	2	4974	25.57	14777	-46.82
IND1 (OF)	3	13731	/	49260	/
IND2 (OF)	3	13778	0.34	48435	-1.67
IND3 (OF)	3	13147	-4.25	45833	-6.96
IND4 (OF)	3	9547	-30.47	33966	-31.05

Table SI-4: $\beta(OF)/\beta(CF)$ **contrast ratios for the static** ($\lambda = \infty$) **and dynamic** ($\lambda = 1064$ **nm) first hyperpolarizabilities, calculated at the M06-2X/6-311G(d) level for the four systems defined in Figure SI-6 (considering three different conformers (Conf.) for the OF). The relative differences (% Diff.) between the contrast values calculated for the IND2-4 systems and the reference IND1 system are also reported.**

		$\lambda = \infty$		$\lambda = 1064$ nm	
System	Conf.	$\beta(OF)/\beta(CF)$	% Diff.	$\beta(OF)/\beta(CF)$	% Diff.
IND1	1	16.14	/	87.30	/
IND2	1	15.46	-4.21	85.53	-2.03
IND3	1	16.02	-0.74	92.06	5.45
IND4	1	26.85	66.37	190.26	117.93
IND1	2	4.68	/	21.28	/
IND2	2	4.52	-3.43	18.94	-10.99
IND3	2	4.94	5.74	18.16	-14.63
IND4	2	14.89	218.45	31.57	48.40
IND1	3	16.21	/	37.72	/
IND2	3	15.69	-3.20	36.55	-3.08
IND3	3	16.50	1.75	38.42	1.86
IND4	3	28.58	76.32	72.58	92.42

Probability distributions of dihedrals

Figures SI-8 and SI-9 report the potential energy curves associated to torsions within the isolated molecule around the $\theta_1 - \theta_{10}$ and $\gamma - \gamma'$ dihedrals, respectively. The plots also show the probability distributions of the dihedral angles for the subset of molecular geometries extracted from the MD trajectories. The distributions indicate that the θ_2 and θ_3 (and in a lesser extent θ_1) dihedrals assume all possible values due to low rotational energy barriers, while all other dihedrals (θ_4–θ_{10}) adopt specific values due to larger energy barriers associated to steric and conjugation constraints.

Relationships between geometrical structures and NLO responses

Figures SI-10 and SI-11 report the scatter plots of β with respect to torsions around $\theta_1 - \theta_{10}$ and $\gamma - \gamma'$ dihedrals, respectively. These graphs evidence how the amplitude of the NLO responses of the molecules within the SAM is strongly correlated to the value of the γ dihedral: large β values are obtained when γ is close to 0° or 180°, while β is much weaker when γ is close to 90°. To gain further insights on the $\gamma - \beta$ relationship, we focused on the three open-form conformers of IND2, since this molecular fragment was selected for the statistical sampling of the NLO properties. As reported in Table SI-3, conformers 1 and 3 display very similar static β values associated to quasi planar conformations with respect to γ, while conformer 2 exhibits a much lower β value associated to a perpendicular conformation. Within the two-state approximation (TSA), the static first hyperpolarizability of these conformers can be expressed as:

$$\beta^{TSA} = 6 \times \frac{\mu_{ge}^2 \Delta\mu_{ge}}{\Delta E_{ge}} = 9 \times \frac{f_{ge}\Delta\mu_{ge}}{\Delta E_{ge}^2} \qquad \text{(SI-1)}$$

in which ΔE_{ge} is the excitation energy between the ground state (g) and the dipole-allowed excited state (e), μ_{ge} is the transition dipole associated to the excitation, $f_{ge} = \frac{2}{3}\Delta E_{ge}\mu_{ge}^2$ is the oscillator strength, and $\Delta\mu_{ge} = |\overrightarrow{\mu_e} - \overrightarrow{\mu_g}|$ is the change in dipole moment between the

two electronic states. This latter quantity can be factorized into two contributions:

$$\Delta\mu_{ge} = \Delta q \times \Delta r \qquad \text{(SI-2)}$$

where Δq is the amount of charge transferred during the excitation, and Δr is the average distance over which this charge transfer occurs. The quantities involved in equations SI-1 and SI-2 were calculated for the three lowest-energy excitations of the IND2 open-form conformers using time-dependent DFT at the M06-2X/6-311G(d) level, and are collected in Table SI-5. Results show that S_2 and S_3 exhibit strong optical absorption (with large oscillator strengths f_{ge}), while the $S_0 \rightarrow S_1$ transition is dipole forbidden with f_{ge} close to zero. Thus, according to equation SI-1, the dark S_1 state does not contribute to the second-order response of the compounds. The differences in the total densities of the optically active S_2 and S_3 states and ground state are reported in Figure SI-12. The density maps show that the lowest-energy $S_0 \rightarrow S_2$ transition is localized on the indolino-oxazolidine moiety and the closest thiophene ring, with no contribution of the central sulfur atom. The most intense $S_0 \rightarrow S_3$ transition is more delocalized and induces an electronic redistribution impacting both the indolino-oxazolidine and bithiophene units. Moreover, in conformers 1 and 3 (showing quasi planar conformations with respect to γ), the charge transfer extends to the central sulfur atom, while this latter does not contribute to the density reorganization in conformer 2 (showing a perpendicular conformation with respect to γ). Therefore, the excitation-induced charge transfer is much more pronounced in planar conformers 1 and 3, with dipole moment variations $\Delta\mu_{ge}$ two times larger than that of conformer 2, mainly due to an increase of the charge transfer distance Δr. In addition, the $S_0 \rightarrow S_3$ transition energies of conformers 2 and 3 are lower than that of conformer 2, which also contributes to increase the β values of these two conformers with respect to conformer 2. The dependence of β on the value of the dihedral angle γ is then explained in terms of the sizable participation of the sulfur atom of the thioalkyl group to the brightest S_3 excitation in the case of planar conformers,

as highlighted in Figure SI-12.

Table SI-5: Excitation energies (ΔE_{ge}, eV), oscillator strengths (f_{ge}), dipole moment variation ($\Delta\mu_{ge}$, D), charge transfer (Δq, |e|) and charge transfer distance (Δr, Å) for the three lowest-energy excitations of the three IND2 open-form conformers.

System (form)	Conf.	Transition	ΔE_{ge}	f_{ge}	$\Delta\mu_{ge}$	Δq	Δr
IND2 (OF)	1	$S_0 \rightarrow S_1$	1.3908	0.0010	9.605	1.013	1.974
		$S_0 \rightarrow S_2$	1.7878	0.3598	3.203	0.470	1.418
		$S_0 \rightarrow S_3$	2.8953	1.2107	7.289	0.538	2.822
IND2 (OF)	2	$S_0 \rightarrow S_1$	1.4396	0.0069	8.194	0.951	1.794
		$S_0 \rightarrow S_2$	1.9202	0.4573	1.548	0.383	0.841
		$S_0 \rightarrow S_3$	3.1123	1.1350	3.774	0.478	1.644
IND2 (OF)	3	$S_0 \rightarrow S_1$	1.4528	0.0043	7.171	0.946	1.578
		$S_0 \rightarrow S_2$	1.8864	0.4223	1.628	0.388	0.874
		$S_0 \rightarrow S_3$	2.9850	1.0865	7.735	0.559	2.879

Origin of the resonance enhancement of the first hyperpolarizability of open forms

To gain insight on the origin of the huge resonance enhancement of the first hyperpolarizability observed for few structures extracted from the open-form SAM layer, the absorption properties of molecules exhibiting the lowest and the largest dynamic β values (respectively referred to as **1** and **2** in the following) were calculated at the M06-2X/6-311G(d) level. The vertical excitation energies and oscillator strengths associated to the lowest-energy optical transitions are reported in Table SI-6 for these two chromophore geometries. Structure **1** with minimal β displays an intense absorption transition ($S_0 \rightarrow S_3$) at 449 nm, as well as a transition ($S_0 \rightarrow S_2$) at 582 nm, associated to a lower oscillator strength. In structure **2** displaying the maximal dynamic β value, the absorption wavelength of the lowest-energy optically-absorbing excited state (S_3) is associated to the largest oscillator strength and red-shifted to 546 nm, *i.e.* very close to the second harmonic wavelength of a 1064 nm laser. This state is thus at the origin of the large resonance-enhancement of the first hyperpolarizability

in this structure.

Table SI-6: Excitation energies (ΔE_{ge}, eV), wavelengths (λ_{ge}, nm) and oscillator strengths (f_{ge}) associated to the lowest-energy dipole-allowed excitations of the open-form molecular structures exhibiting the lowest (1) and largest (2) dynamic β values (in a.u.).

Structure	β	Transition	ΔE_{ge}	λ_{ge}	f_{ge}
1	3295	$S_0 \rightarrow S_2$	2.1302	582	0.3611
		$S_0 \rightarrow S_3$	2.7585	449	0.8995
		$S_0 \rightarrow S_5$	3.6252	342	0.1236
2	$>10^{11}$	$S_0 \rightarrow S_3$	2.2718	546	0.8026
		$S_0 \rightarrow S_4$	2.9335	423	0.3023
		$S_0 \rightarrow S_5$	3.2863	377	0.2020

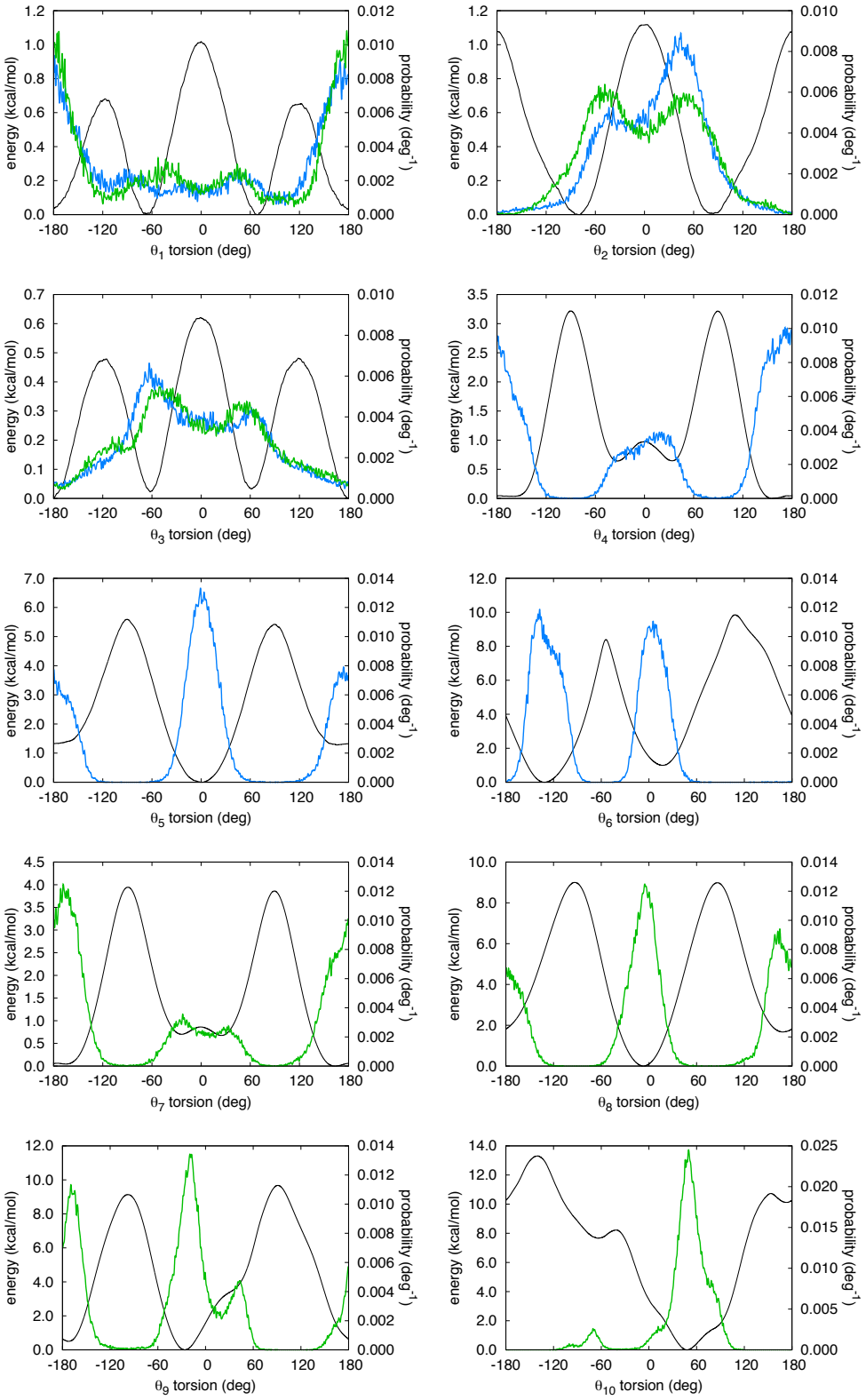

Figure SI-8: Potential energy curves associated to torsions $\theta_1 - \theta_{10}$ (black line) and probability distributions of the dihedral angles of molecules in the SAM, in the closed (blue) and open (green) forms.

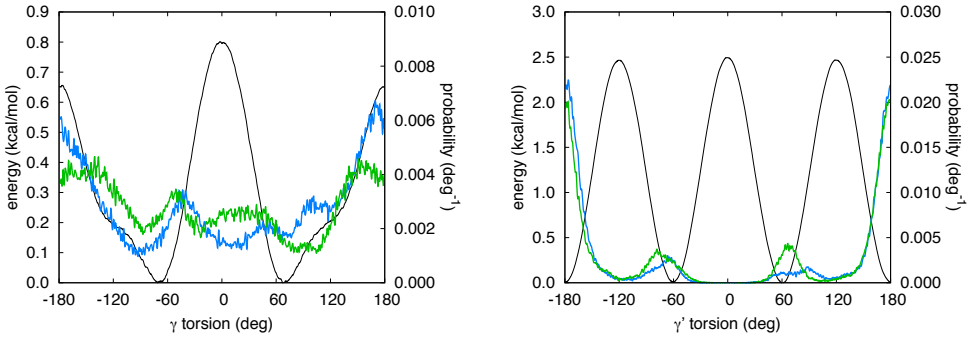

Figure SI-9: Potential energy curves associated to torsions γ and γ' (black line) and probability distributions of the dihedral angles of molecules in the SAM, in the closed (blue) and open (green) forms.

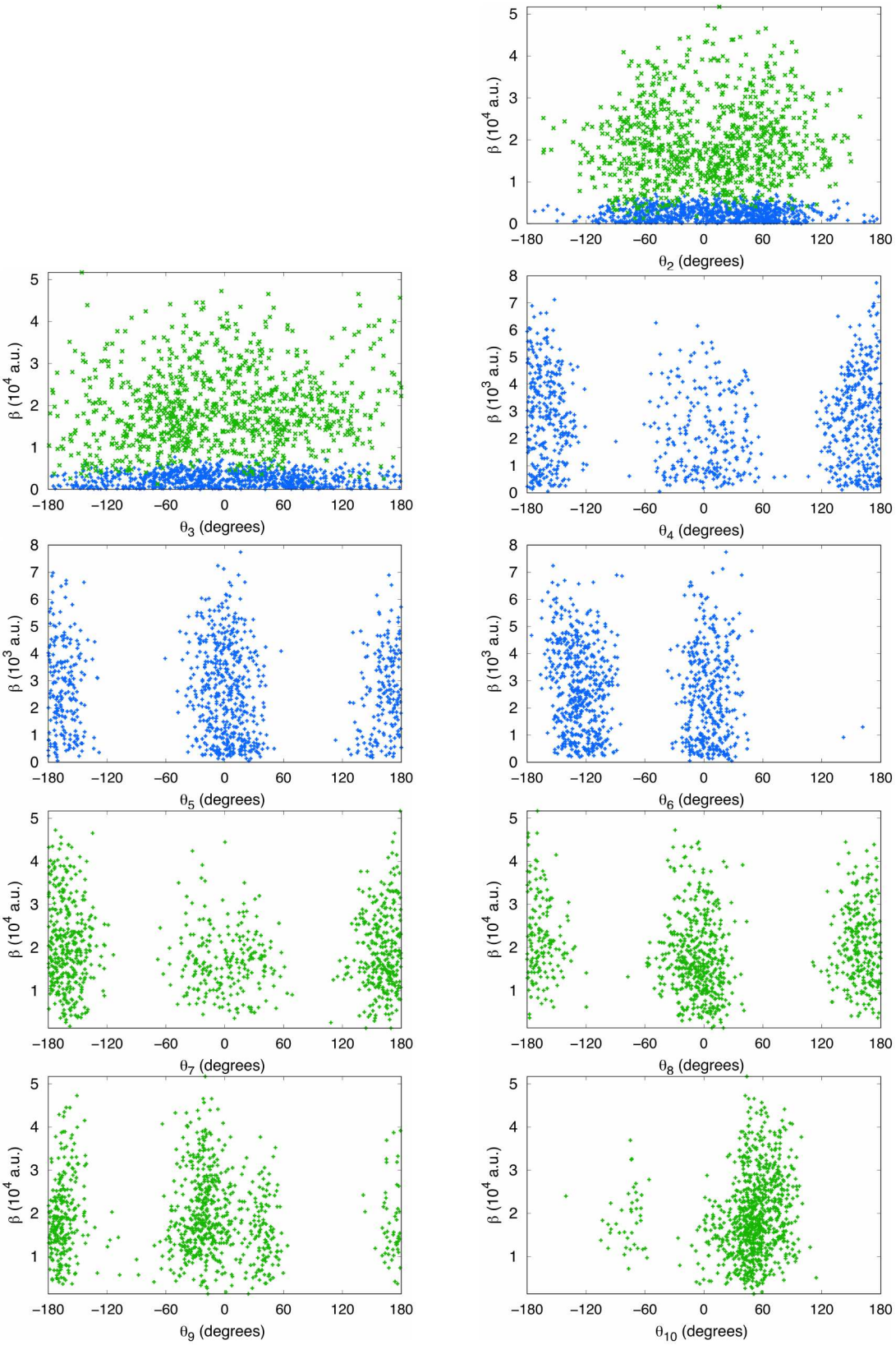

Figure SI-10: Scatter plots of individual values of β with respect to torsion angles $\theta_2 - \theta_{10}$ for molecules in closed (blue) and open (green) forms.

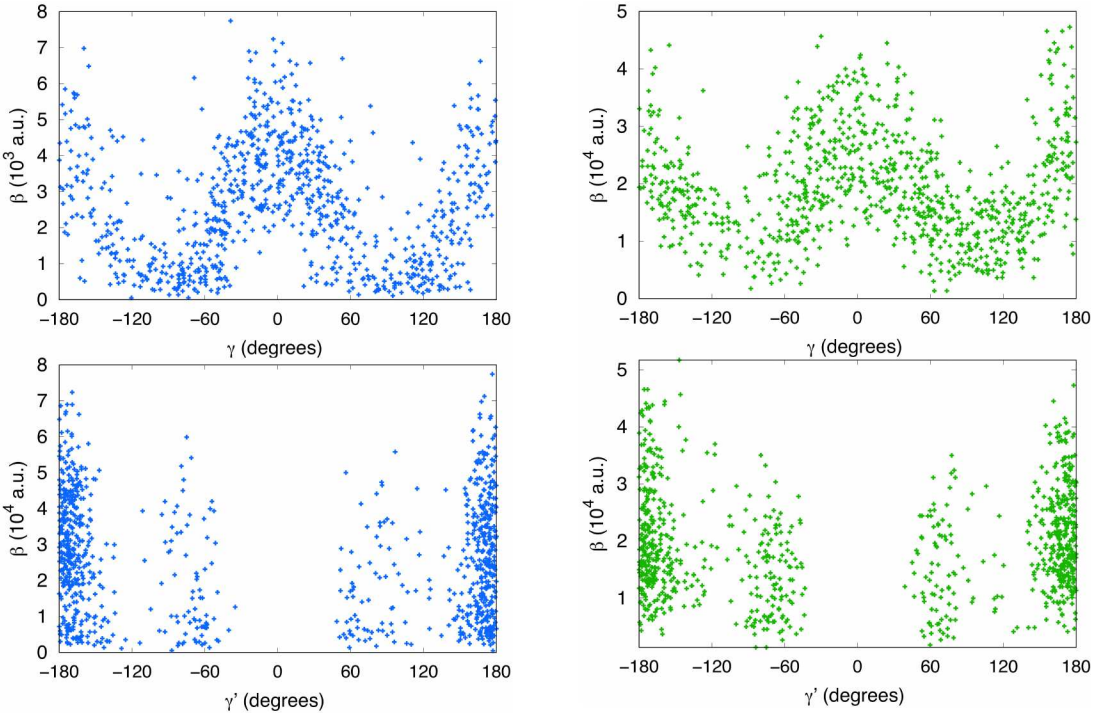

Figure SI-11: Scatter plots of individual values of β with respect to torsion angles γ and γ' for molecules in closed (blue) and open (green) forms.

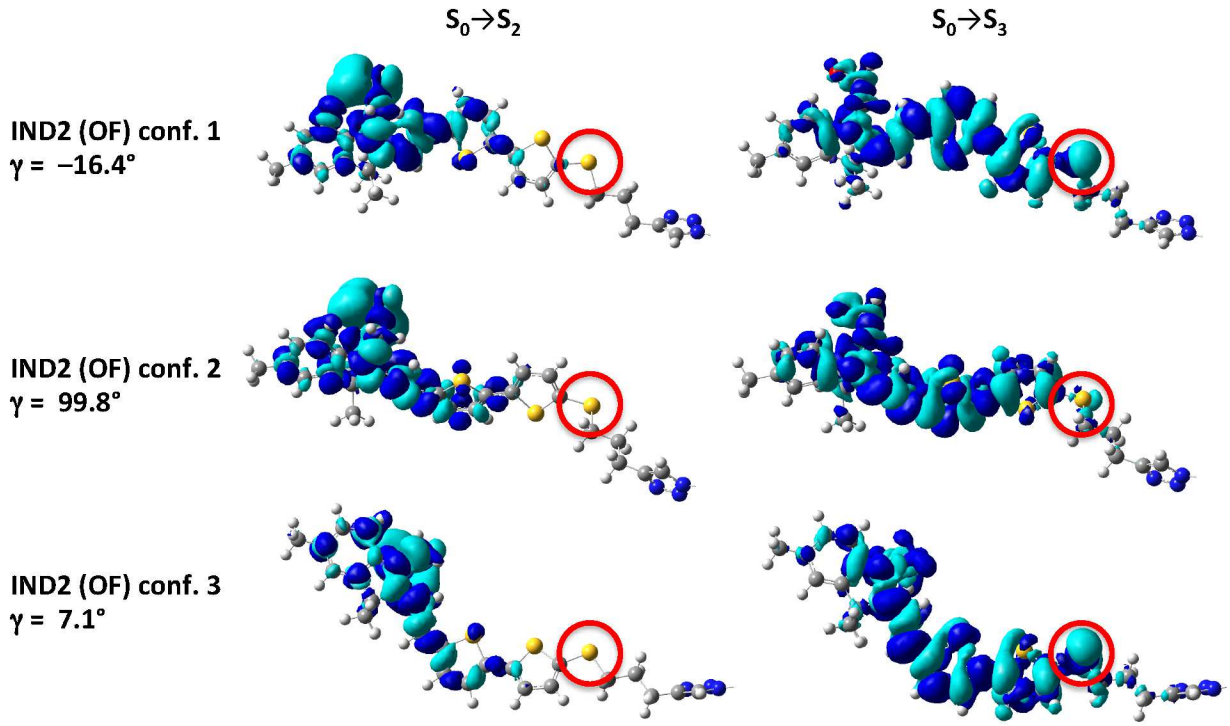

Figure SI-12: Density difference maps calculated at the M06-2X/6-311G(d) for the three IND2 open-form conformers (isovalues = 0.0004). Light (dark) blue lobes are associated with negative (positive) values. The terminal alkyl chains are hidden for clarity. The red circles highlight the contribution of the thioalkyl sulfur atom in the electronic redistribution.

References

(S1) Cygan, R. T.; Liang, J.-J.; Kalinichev, A. G. Molecular Models of Hydroxide, Oxyhydroxide, and Clay Phases and the Development of a General Force Field. *J. Phys. Chem. B* **2004**, *108*, 1255–1266.

(S2) Valle, R. G. D.; Andersen, H. C. Molecular dynamics simulation of silica liquid and glass. *J. Chem. Phys.* **1992**, *97*, 2682–2689.

(S3) Martínez, L.; Andrade, R.; Birgin, E. G.; Martínez, J. M. PACKMOL: A package for building initial configurations for molecular dynamics simulations. *J. Comput. Chem.* **2009**, *30*, 2157–2164.

(S4) Mozzi, R. L.; Warren, B. E. The structure of vitreous silica. *J. Appl. Crystallogr.* **1969**, *2*, 164–172.

(S5) Feuston, B. P.; Garofalini, S. H. Topological and bonding defects in vitreous silica surfaces. *J. Chem. Phys.* **1989**, *91*, 564–570.

(S6) Mityashin, A.; Roscioni, O. M.; Muccioli, L.; Zannoni, C.; Geskin, V.; Cornil, J.; Janssen, D.; Steudel, S.; Genoe, J.; Heremans, P. Multiscale Modeling of the Electrostatic Impact of Self-Assembled Monolayers used as Gate Dielectric Treatment in Organic Thin-Film Transistors. *ACS Appl. Mater. Interfaces* **2014**, *6*, 15372–15378.

(S7) Pielak, K.; Bondu, F.; Sanguinet, L.; Rodriguez, V.; Champagne, B.; Castet, F. Second-Order Nonlinear Optical Properties of Multiaddressable Indolinooxazolidine Derivatives: Joint Computational and Hyper-Rayleigh Scattering Investigations. *J. Phys. Chem. C* **2017**, *121*, 1851–1860.

Atomic coordinates of the reference IND1 molecule

IND1 closed form

C	11.06435100	1.94829900	-0.62034400
C	10.51681700	2.98303200	0.13306200
C	11.13203500	4.21461700	0.17974200
C	12.32284600	4.43231900	-0.52165400
C	12.85276900	3.38438000	-1.26597100
C	12.23609800	2.13692300	-1.32962700
H	10.69989800	5.02589200	0.76907700
H	13.77868700	3.54431900	-1.81761400
H	12.66825200	1.34060200	-1.93275200
C	12.99854400	5.76815000	-0.46436800
H	12.35565800	6.56455800	-0.85942000
H	13.25364300	6.04874600	0.56500200
H	13.92567300	5.77761600	-1.04618400
C	9.21499900	2.52271400	0.73547800
C	9.00570500	2.94531800	2.17879100
H	8.88572100	4.03366800	2.24213100
H	8.09379200	2.49416100	2.58996600
H	9.84610600	2.64833700	2.80951900
C	8.06750400	3.04181100	-0.13122600
H	8.15718100	2.70217800	-1.16918900
H	7.09276900	2.71405800	0.24873600
H	8.07990900	4.13820100	-0.13531000
C	9.37076800	0.98196900	0.58917100
C	8.08752000	0.22043200	0.49588700
H	7.57088800	0.11205700	1.45243200
C	7.58382000	-0.30399700	-0.62171300
H	8.14477300	-0.16733400	-1.55003800
C	6.35289900	-1.04405500	-0.75520200
C	5.84844400	-1.58620600	-1.90788100
S	5.27921100	-1.35179100	0.58318300
C	4.62274800	-2.25828500	-1.73162500
H	6.36640000	-1.50307500	-2.85978300
C	4.17301200	-2.23359800	-0.43774700
H	4.09008600	-2.76923400	-2.52915800
C	2.97142600	-2.80888600	0.11472700
C	2.69961400	-3.13295900	1.41992500
S	1.61049600	-3.17927100	-0.90580000
C	1.40827100	-3.66892500	1.60878600
H	3.42477000	-3.00324000	2.21910600
C	0.68657200	-3.76355100	0.45258800
H	1.00876800	-3.99104400	2.56589800
S	-0.93681700	-4.40045900	0.24824100
C	-1.87017100	-2.82148400	0.13980400
H	-1.63678100	-2.22768300	1.03213000
H	-1.51761000	-2.26716300	-0.73876900
C	-3.35167400	-3.10978800	0.03935400
H	-3.56130200	-3.73766200	-0.83676500
H	-3.68531000	-3.68189600	0.91703700
C	-4.16390200	-1.82361800	-0.07101100
H	-3.98415500	-1.18822800	0.80754100
H	-3.81508100	-1.25213000	-0.94337000
C	-6.66024400	-1.80380400	0.63512600
H	-6.71635600	-1.31557200	1.59865400
C	-5.61973900	-2.08567600	-0.21224400
N	-6.12918400	-2.72220700	-1.29989600
N	-7.41227500	-2.84067500	-1.16858100
N	-7.75093100	-2.29647000	0.00674600

C	-9.14744200	-2.17661100	0.37692600
H	-9.66637000	-3.01966800	-0.09215000
H	-9.22644800	-2.30159500	1.46442700
C	-9.73857600	-0.85415100	-0.07048900
H	-9.61141700	-0.76682600	-1.15916400
H	-9.15908500	-0.02930400	0.37241200
C	-11.20202800	-0.71970500	0.30429400
H	-11.77507300	-1.54947800	-0.13965600
H	-11.31752700	-0.82937600	1.39507200
C	-11.80093200	0.60297700	-0.13612200
H	-11.21765600	1.43051200	0.29937300
H	-11.69140400	0.70835800	-1.22726600
C	-13.26107200	0.76218000	0.24414100
H	-13.84841700	-0.05926300	-0.19738500
H	-13.37041600	0.64967600	1.33521300
C	-13.84691700	2.09347000	-0.18721500
H	-13.25206400	2.91243600	0.24923600
H	-13.74201000	2.20415800	-1.27870700
C	-15.30349200	2.26915800	0.19988600
H	-15.90263400	1.45731400	-0.24388400
H	-15.40955500	2.15089300	1.29071300
C	-15.87651700	3.60959700	-0.22037300
H	-15.27399300	4.41962200	0.22195400
H	-15.77196100	3.72830500	-1.31109900
C	-17.33110500	3.79553700	0.16897000
H	-17.93885300	2.99272400	-0.27995300
H	-17.43917400	3.67286300	1.25928500
C	-17.89179600	5.14451300	-0.24311400
H	-17.28622100	5.94598000	0.20476700
H	-17.78579900	5.26796900	-1.33204800
C	-19.35399200	5.33402500	0.14886200
H	-19.95802000	4.55271900	-0.31245300
H	-19.45009700	5.27508300	1.23301500
C	10.95882600	-0.46192900	-0.24736300
H	11.91443700	-0.51592600	-0.77440600
H	10.34540000	-1.31089300	-0.56623900
C	11.10511600	-0.41091700	1.27560200
H	12.08360800	-0.00622300	1.57106500
H	10.97892000	-1.39545400	1.74247200
O	10.09294900	0.47070000	1.72153600
N	10.26203200	0.78287400	-0.55352700
H	-19.69853100	6.30967200	-0.19392900

IND1 open form, conformer 1

C	11.59577700	1.28003600	-0.84863100
C	11.63100600	-0.00716800	-1.36006100
C	12.81436800	-0.52135400	-1.84480700
C	13.96881500	0.26595100	-1.80108200
C	13.90125500	1.54289700	-1.24108900
C	12.71803500	2.08203400	-0.75153400
H	12.86238500	-1.53441800	-2.24712700
H	14.81468600	2.13118900	-1.16910600
H	12.67385700	3.02548100	-0.21109800
C	15.26051600	-0.25453000	-2.35049200
H	15.33862500	-1.34186800	-2.24439000
H	15.35703100	-0.02822400	-3.42020300
H	16.12351800	0.19412000	-1.84826700
C	10.26785200	-0.62277500	-1.22545100
C	9.67001400	-0.92942100	-2.60095400
H	10.29426800	-1.66660200	-3.11905500

H	8.65985000	-1.34734100	-2.52129500
H	9.62384800	-0.02985300	-3.22439100
C	10.30348800	-1.88003200	-0.35910700
H	10.72290500	-1.66604700	0.62937600
H	9.29998000	-2.29932100	-0.22261100
H	10.92724100	-2.64682200	-0.83354700
C	9.49720600	0.49718800	-0.54695100
C	8.14178500	0.36145700	-0.17962700
H	7.62841700	-0.46744500	-0.67244700
C	7.44499300	1.06630300	0.75802400
H	7.97143000	1.78521600	1.38552800
C	6.07737100	0.88914400	1.09506000
C	5.40777900	1.51361400	2.12661400
S	4.99756000	-0.19225300	0.24083200
C	4.06994200	1.12265500	2.25372700
H	5.90019700	2.22931600	2.77926400
C	3.67980000	0.19169900	1.31681500
H	3.40132400	1.49409900	3.02516900
C	2.39903100	-0.43408500	1.15390200
C	2.05582000	-1.52213800	0.39585000
S	0.99451300	0.18206300	1.99868800
C	0.69757000	-1.88888200	0.49835700
H	2.77548200	-2.07048900	-0.20662200
C	-0.01171700	-1.07293400	1.33880800
H	0.26678300	-2.73978300	-0.01849800
S	-1.69337000	-1.11648100	1.82688100
C	-2.37864100	-2.21912700	0.54726200
H	-2.07842600	-1.83655600	-0.43668100
H	-1.95525100	-3.22341000	0.67426500
C	-3.88633500	-2.26041900	0.68579300
H	-4.16959700	-2.61578700	1.68504300
H	-4.30201100	-1.24822100	0.58558500
C	-4.51541700	-3.17818700	-0.35635100
H	-4.28550800	-2.81581500	-1.36810100
H	-4.06527800	-4.17852500	-0.27514300
C	-7.01493000	-2.94313900	-1.02071700
H	-7.04662900	-2.51322500	-2.01269000
C	-5.98722400	-3.29102200	-0.18230300
N	-6.53047400	-3.79995700	0.95465100
N	-7.82168700	-3.78684200	0.85852500
N	-8.13337000	-3.27773200	-0.33937100
C	-9.52179800	-3.06938500	-0.70203800
H	-9.62794200	-3.26614600	-1.77651600
H	-10.09770700	-3.83295800	-0.16781700
C	-10.00717800	-1.67721700	-0.34817700
H	-9.38200400	-0.92990400	-0.86076200
H	-9.85701100	-1.51701100	0.72909700
C	-11.46524100	-1.47790200	-0.71562300
H	-11.60414800	-1.66544500	-1.79300900
H	-12.08056000	-2.23387800	-0.20188100
C	-11.98188400	-0.09204900	-0.37594600
H	-11.84890800	0.09497200	0.70149900
H	-11.36441300	0.66506800	-0.88583600
C	-13.43871400	0.10703200	-0.75000700
H	-13.56932400	-0.08680400	-1.82725400
H	-14.05536800	-0.64948500	-0.23798000
C	-13.96296600	1.49229000	-0.42048000
H	-13.83845000	1.68591300	0.65724000
H	-13.34417000	2.24944500	-0.92911900
C	-15.41774400	1.68823800	-0.80444000

H	-15.54097400	1.49085700	-1.88194900
H	-16.03657600	0.93196300	-0.29440800
C	-15.94652200	3.07347300	-0.48204500
H	-15.82844700	3.27074600	0.59574700
H	-15.32646800	3.83051600	-0.98924900
C	-17.39942700	3.26737300	-0.87361000
H	-17.51876000	3.07058900	-1.95179000
H	-18.02198000	2.51265400	-0.36541400
C	-17.92808800	4.65369400	-0.55250900
H	-17.81318700	4.85114700	0.52352200
H	-17.30739700	5.40875400	-1.05946600
C	-19.38840400	4.84575300	-0.95104400
H	-19.49940800	4.67251800	-2.03163100
H	-20.01625300	4.13108800	-0.39872100
C	9.93610500	2.87203200	0.06358300
H	8.85297500	3.01321900	-0.00917100
H	10.45139100	3.61666200	-0.55003400
C	10.44288400	3.12521600	1.58929800
H	9.90617700	2.30575900	2.16100000
H	9.87120800	4.07506300	1.81418300
O	11.72275000	3.16422600	1.69757900
N	10.27475100	1.57567100	-0.42870400
H	-19.70230200	5.87210900	-0.71008600

IND1 open form, conformer 2

C	11.15614100	1.49734900	-1.24424800
C	11.61169200	0.22719800	-0.93712400
C	12.91649500	-0.12676600	-1.21347200
C	13.76807900	0.80758100	-1.80280800
C	13.28480000	2.09123900	-2.07225600
C	11.98057700	2.46384000	-1.79414200
H	13.29116000	-1.12070200	-0.96605700
H	13.96497000	2.82723900	-2.49858100
H	11.64350400	3.48007500	-1.96020600
C	15.18296500	0.45525200	-2.14084500
H	15.47686900	-0.50616000	-1.70839600
H	15.32923800	0.38504300	-3.22604300
H	15.88333700	1.21426400	-1.77441300
C	10.52502500	-0.51741600	-0.21251200
C	10.24704000	-1.87620700	-0.84470000
H	11.15370200	-2.49148400	-0.81554700
H	9.45841500	-2.42844600	-0.32520000
H	9.94828500	-1.76903200	-1.89301100
C	10.94337300	-0.62940500	1.26318400
H	11.15595400	0.36614500	1.67086800
H	10.16445700	-1.09484500	1.87618100
H	11.85362800	-1.23476300	1.34688400
C	9.37237400	0.46295100	-0.31146800
C	8.04056900	0.27946600	0.11302500
H	7.34634300	1.08257700	-0.13627000
C	7.54246800	-0.78860600	0.79495600
H	8.20775100	-1.59074500	1.11344900
C	6.18528400	-0.97558700	1.17737400
C	5.67689300	-2.03532400	1.89975000
S	4.90587000	0.14111100	0.76281000
C	4.29777500	-1.95283600	2.13321600
H	6.30846500	-2.84367500	2.25842600
C	3.71908600	-0.82857500	1.59258200
H	3.73393400	-2.68364100	2.70620000
C	2.34156300	-0.41482900	1.63279800

C	1.82160400	0.84285300	1.44700700
S	1.07039100	-1.56545500	1.94039000
C	0.41655700	0.88898800	1.54483500
H	2.44391300	1.71560500	1.26759300
C	-0.14886300	-0.32767000	1.80769300
H	-0.17888100	1.79069500	1.43780800
S	-1.85169400	-0.69352700	2.03021100
C	-2.24036500	-1.35775500	0.36080900
H	-1.93481900	-0.60950500	-0.38084200
H	-1.64436500	-2.26388400	0.19649300
C	-3.72016900	-1.65673300	0.26723200
H	-4.01304900	-2.38312700	1.03707600
H	-4.30143600	-0.74467900	0.46528400
C	-4.09575700	-2.21279900	-1.10275300
H	-3.83243000	-1.48977400	-1.88739500
H	-3.50269100	-3.11710400	-1.30027700
C	-6.55245500	-1.96424700	-1.90436200
H	-6.58150800	-1.13674400	-2.60025500
C	-5.54026200	-2.55056300	-1.18878900
N	-6.07657900	-3.56982900	-0.46673600
N	-7.34840600	-3.64096500	-0.70056600
N	-7.65313000	-2.67851100	-1.57957000
C	-9.03347200	-2.45199100	-1.96072100
H	-9.05703700	-2.17100000	-3.02146400
H	-9.54212700	-3.41720600	-1.86279100
C	-9.69627300	-1.39674700	-1.09719900
H	-9.13294500	-0.45405000	-1.17658600
H	-9.62211600	-1.70995700	-0.04579800
C	-11.14586400	-1.17108500	-1.48143400
H	-11.20832000	-0.87865300	-2.54245700
H	-11.70001200	-2.12023800	-1.40281900
C	-11.82595700	-0.11681200	-0.62780900
H	-11.76458800	-0.41009000	0.43234400
H	-11.26892100	0.83114500	-0.70387000
C	-13.27617800	0.11709000	-1.00660500
H	-13.33665500	0.40604500	-2.06864900
H	-13.83390600	-0.83028600	-0.92717100
C	-13.95465200	1.17548100	-0.15708700
H	-13.89557100	0.88638000	0.90475200
H	-13.39523400	2.12207500	-0.23524800
C	-15.40420800	1.41337100	-0.53637800
H	-15.46328600	1.69874500	-1.59951200
H	-15.96498200	0.46785400	-0.45439500
C	-16.08057300	2.47656100	0.30889600
H	-16.02212300	2.19235200	1.37207400
H	-15.51994000	3.42204400	0.22661300
C	-17.52978100	2.71553500	-0.07059200
H	-17.59059400	2.99561000	-1.13518200
H	-18.09475500	1.77296100	0.01872200
C	-18.20128300	3.78602100	0.77047400
H	-18.14138000	3.51117000	1.83373900
H	-17.64083400	4.72928300	0.67735200
C	-19.65918300	4.02216100	0.38856100
H	-19.71861400	4.30923500	-0.67165400
H	-20.23499100	3.09915000	0.55134100
C	9.17307900	2.86884200	-0.81526100
H	8.08441200	2.79222400	-0.80717800
H	9.49878700	3.48996300	-1.65202900
C	9.66340000	3.56066500	0.59771100
H	9.10409400	2.87533900	1.31256900

H	9.09905600	4.53652300	0.57116300
O	10.93571000	3.59965600	0.71602500
N	9.79454800	1.59750900	-0.88687700
H	-20.07521400	4.82837400	1.01060600

IND1 open form, conformer 3

C	10.60823400	2.77990600	-0.05179500
C	11.41519800	1.74437600	-0.49351900
C	12.75495400	1.96041500	-0.73237600
C	13.28996900	3.23505800	-0.53311200
C	12.45634200	4.25173800	-0.06532900
C	11.10925700	4.04540600	0.19124400
H	13.40284400	1.14705100	-1.06227800
H	12.88373100	5.23552300	0.12176000
H	10.49472900	4.84001100	0.59956300
C	14.73220400	3.50605800	-0.82720800
H	15.35961400	2.63301300	-0.61776900
H	14.88227600	3.76298300	-1.88385900
H	15.11575300	4.34279200	-0.23471300
C	10.61108600	0.47462400	-0.50281300
C	10.74768900	-0.28742600	-1.81348800
H	11.79933200	-0.54262300	-1.98728900
H	10.18143300	-1.22318300	-1.81884900
H	10.40524700	0.31769300	-2.65994900
C	11.06253500	-0.34785900	0.71954600
H	10.96907700	0.25973300	1.62837400
H	10.46695800	-1.25862300	0.84341700
H	12.11373900	-0.63645800	0.60163800
C	9.22059900	0.99960400	-0.20478400
C	8.00555100	0.28495800	-0.19881800
H	7.10320500	0.88128100	-0.05802200
C	7.85427600	-1.05945400	-0.35699200
H	8.73373600	-1.69717000	-0.44075100
C	6.62349700	-1.76788800	-0.39895300
C	6.46994900	-3.13526900	-0.50463400
S	5.05809200	-0.99135300	-0.33353900
C	5.13559500	-3.55967300	-0.50929200
H	7.32332600	-3.80657400	-0.55486200
C	4.23314700	-2.52372800	-0.42145400
H	4.82636500	-4.60005200	-0.54366200
C	2.79826200	-2.61248400	-0.42657100
C	2.02210400	-3.61798300	-0.93674200
S	1.79219300	-1.37433100	0.29291000
C	0.63553700	-3.41160000	-0.77276200
H	2.44379400	-4.47710500	-1.45107200
C	0.34357200	-2.23494100	-0.13508700
H	-0.11801000	-4.10422500	-1.13202900
S	-1.19591800	-1.51422300	0.29127500
C	-2.32071400	-2.87476100	-0.15543600
H	-2.24369800	-3.05755100	-1.23526200
H	-1.99936000	-3.78110500	0.37331300
C	-3.73820200	-2.50484000	0.22895300
H	-3.81050900	-2.34304500	1.31181400
H	-4.02900100	-1.55811700	-0.24790100
C	-4.71752800	-3.60171600	-0.17313100
H	-4.71764600	-3.72902200	-1.26468500
H	-4.37580100	-4.55881200	0.24868100
C	-7.27440400	-3.19904200	-0.38938700
H	-7.52120300	-3.24686200	-1.44121700
C	-6.09875600	-3.33033600	0.30418400

N	-6.37593800	-3.18268900	1.62667400
N	-7.64491600	-2.97458000	1.77978200
N	-8.20727700	-2.98977700	0.56588800
C	-9.62676100	-2.72957200	0.42325300
H	-9.99481200	-3.31204300	-0.43090200
H	-10.10549600	-3.12833300	1.32446500
C	-9.93663400	-1.25465100	0.25821100
H	-9.42736400	-0.86878900	-0.63820600
H	-9.51167500	-0.71015300	1.11346000
C	-11.42987500	-1.00742900	0.16204900
H	-11.84609000	-1.57585100	-0.68588000
H	-11.92471600	-1.41155800	1.05979200
C	-11.78982600	0.45905700	0.00988100
H	-11.36728100	1.02926100	0.85244400
H	-11.30822700	0.86564800	-0.89393200
C	-13.28684200	0.69404100	-0.06125500
H	-13.70785100	0.12337400	-0.90516800
H	-13.76370200	0.27858700	0.84135200
C	-13.66690600	2.15647400	-0.20134700
H	-13.24222600	2.72828600	0.63961700
H	-13.19932400	2.57410300	-1.10772500
C	-15.16666200	2.37883200	-0.25636000
H	-15.59044800	1.81062600	-1.10057900
H	-15.63170800	1.95242800	0.64742700
C	-15.55974400	3.83911100	-0.38232200
H	-15.13541300	4.40781600	0.46092200
H	-15.10034400	4.26816800	-1.28753000
C	-17.06108800	4.05202700	-0.42834200
H	-17.48657200	3.49005400	-1.27603600
H	-17.52117700	3.61698500	0.47409400
C	-17.45998300	5.51254800	-0.53961100
H	-17.03828000	6.07518500	0.30619100
H	-17.00560300	5.95027400	-1.44181800
C	-18.97114600	5.71760300	-0.58148500
H	-19.39021200	5.18083200	-1.44534800
H	-19.41972900	5.32882200	0.34459500
C	8.36006900	3.02352800	0.89415900
H	7.32673100	2.74237400	0.68068400
H	8.49285100	4.09666100	0.74485000
C	8.71462000	2.61599900	2.45030800
H	8.32483900	1.54707300	2.41945900
H	7.96185200	3.22127100	3.03036900
O	9.95479600	2.75951900	2.73397200
N	9.28696900	2.30510500	0.09143800
H	-19.19309800	6.79100800	-0.67389200

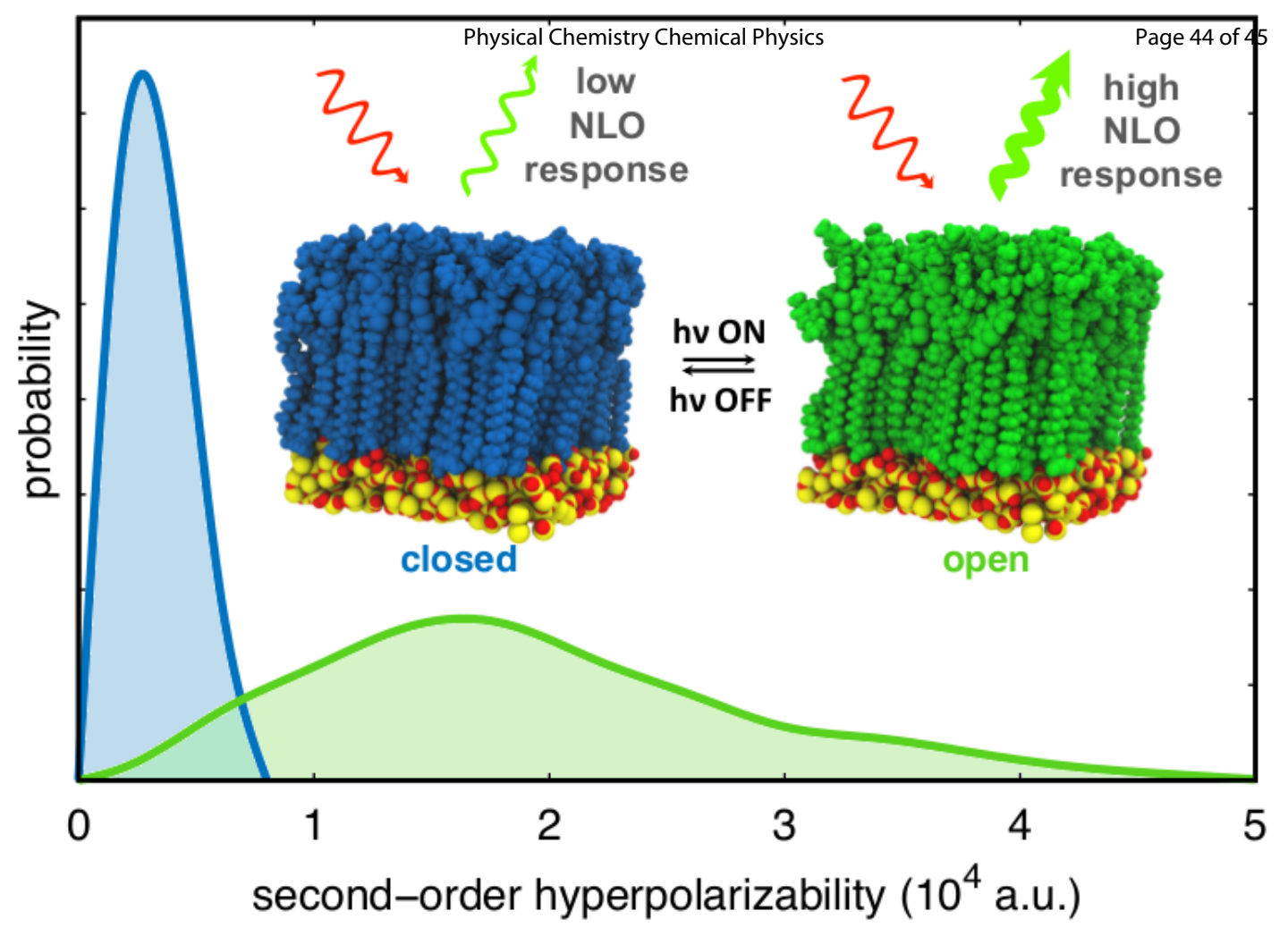
low
NLO
response
high
NLO
response
hv ON
hv OFF
closed
open
probability
0
1
2
3
4
5
second–order hyperpolarizability (10^4 a.u.)

The second harmonic generation responses of photoresponsive self-assembled monolayers based on indolino-oxazolidine derivatives are computed using a sequential MD/DFT approach.